Reduced carbonic fluid and possible nature of high K magmas of Tolbachik.

Alexander Simakin (1,2), Tamara Salova (1), Vera Devyatova (1) and Michael Zelensky (1),
(1) Institute of Experimental Mineralogy RAS, Thermodynamics of minerals, Chernogolovka, Russian Federation
(simakin@iem.ac.ru)
(2) Institute of Earth Physics (IEP) RAS, Moscow

Abstract

Historical basaltic eruptions of Tolbachik volcano (Kamchatka) are of a medium to high potassic type. The potassic character of magmatism can be attributed to the influence of CO_2 – CO rich fluid at or near the magma generation depths. Decarbonatization reactions in the mantle under Tolbachik producing a column of the carbonic fluids may be connected with the recent accretion of Kronotsky paleo-arc with carbonates dragged under the mantle wedge. With thermodynamic modelling we show that reduced carbonic fluid at fO_2 <NNO may be a good carrier of nickel transported in the form of $Ni(CO)_4$. This carbonyl is expected to become thermally stable near the magmatic temperatures at pressures above 1 GPa. In the crust it is predicted to be thermally stable within the PT field of the amphibolite facies. We connect the particles of native Ni and Ag-Pt alloy observed in the volcanic aerosols from the 2012-13 Tolbachik eruption with flushing of the ascending Tolbachik magma with reduced carbonic fluids enriched with PGE and Ni. Native metals may form by the thermal decomposition of the carbonyls and other carbon-bearing compounds dissolved in the fluid.

Introduction

Native metals (Fe, Ag, Cu, Zn, Cu, Pb, Sn and their alloys) have been reported in different products of Kamchatka volcanoes: airfall tephra, pyroclastic deposits, rocks of fumaroles (Glavatskih, 1990; Glavatskikh and Trubkin, 2000; Karpov and Mokhov, 2004). Native metals Ni and Fe-Cr alloy have been found in the mantle xenoliths at the Avacha volcano (SE Kamchatka) (Ishimaru et al., 2009). It is generally accepted that some reducing fluids of the system C-O-H such as H_2, CH_4 and CO are responsible for the native metals formation (Dekov and Damyanov, 1996). Some researchers prefer hydrogen since it is firmly established that native metals in serpentinites are reduced by the secondary hydrogen produced by the reaction of olivine and orthopyroxene with water. Hydrogen is assumed to leave the zone of serpentinization and to reach somehow magma generation level away from the forearc (Ishimaru

et al., 2009). On the other hand, in many cases carbides of metals are reported in pyroclastic deposits (Fe_3C - Grebennikov et al.,2012) and in the deep mantle settings (SiC, CrC) along with diamond, graphite and native metals (Bai et al., 2000) pointing to the involvement of carbon in the origin of the native metals. . Thermodynamic modelling predicts that oxygen fugacity of CCO buffer drops below IW at low P and high T and creates conditions favorable for the formation of native iron (Iacono-Marziano et al., 2012) and less electronegative elements (Cu, Z, Pb). The general problem concerning rare metals with rather low background contents (Ni, PGE, Au etc.) is to concentrate them and produce metal particles of the appreciable size (up to tens of microns). Formation of the volatile (or soluble) forms of these metals is required for metal extraction, transport and accumulation. The ability of the dry fluid of C-O-S composition containing CO, COS, CS_2 to transport Ni and PGE is suspected based on the physico-chemical arguments (Simakin, 2014a). Volatile carbonyls of Co and Ni are assumed to be sufficiently stable to become geologically significant (Teague et al., 2011).

Recently the link between the carbonic fluids in the mantle and formation of potassic low silica magmas was firmly established based on generalized experimental and petrologic observations (Gupta, 2015). In the subduction setting formation of potassium rich magmas is connected with partial melting of a mantle metasomatized by carbonic fluid generated from $CaCO_3$-rich sediments (Conticelli et al., 2010; Nikogosian and van Bergen, 2010). In Italy a zone of high-K magmatism extends from Tuscany to Compania and exactly coincides with an area of the high diffusive CO_2 flux (Frezzotti et al., 2009). No high surface CO_2 flux is detected in Aeolian arc and the potassium content of Aeolian lavas is not as high as in continental Italy (Frezzotti et al., 2009; Peccerillo et al., 2013). However, CO_2 fluxing has also been observed at Stromboli (Cortes et al., 2006). Nikogosian and van Bergen (2010) analyzed numerous melt inclusions in olivine from the volcanic rocks of the central Italy and found that potassium content is positively correlated with decreasing fO_2 (variation in the range NNO-1.5 to NNO+0.5). They argue that reduced carbonic fluid is responsible for the highest potassium enrichment. The appearance of carbonic fluid in the mantle or lower crust (near Moho boundary) is explained by reactions of carbonates with silicates (silica, olivine) at the pressures below 2 GPa (depth < 60-70 km) while carbonatitic melt is stable in association with eclogite and peridotite at P > 2-3 GPa (see in Frezzotti et al., 2009) or depth 80-100 km.

In Kamchatka potassic basalts in subduction settings can also be connected with effect of the carbonated mantle. In the Pliocene potassic volcanism started in the Central Kamchatka (Sredinny) Ridge and continues until now. Basaltic magmas erupted by Plosky and Tolbachik volcanoes (Klyuchevskaya group or KGV) also have a high potassium content. Ponamareva et al. (2013) estimate that the volume of high-K early Holocene pyroclastics of Plosky volcano is

ca 10 km^3. In 2012-2013 Tolbachik volcano erupted lavas containing up to 2.5-3.5 wt.% K_2O. They have all attributes of high-K magmas such as high Ba (600 ppm) and Zr (250 ppm) contents (Volynets et al., 2013). The KGV is in a typical subduction setting with distance from the trench 250-270 km and to the subducting slab 150-180 km (Seliverstov, 2007). Currently subducting sediments in Kurilo-Kamchatka subdution zone are rather poor in carbon and some effective geodynamic mechanism providing mantle wedge fertilization with carbon is required.
In this paper we describe the findings of native metals (Fe, Ni, Ag-Pt) in the Tolbachik 2012-2013 aerosols made by one of us (M. Zelensky). Conditions of the deep Tolbachik magma evolution are illuminated with our data on the Ol and Cpx phenocrysts from the 1941 eruption volcanic bomb and their melt inclusions. The thermodynamic analysis of the stability of $Ni(CO)_4$ and COF_2 as possible important components of a reduced carbonic fluid allows us construct model for the formation of Tolbachik magma.

Petrologic observations.

During the Holocene Tolbachik volcano periodically has erupts magma with composition between high magnesian (HMB) with MgO up to 10 wt.%, Al_2O_3 ≈13 wt.% and high alumina with Al_2O_3= 16-17 wt.%, MgO= 4-6 wt.% basalts (HAB) (Braitseva et al., 1984; Flerov et al., 1984). Both varieties have significant potassium contents (see Table 1 and Fig.1). During the Great Fissure Eruption of 1975-1976, HAB and HMB were erupted from the separated Northern and Southern vent areas respectively. The recent fissure eruption of the 2012-2013 produced HAB flows. The small 1941 eruption erupted lava close to HMB with high explosivity. It was suggested that HAB is a product of the fractional crystallization of HMB (Lukanin et al., 1980). This hypothesis problematic because on the SiO_2-K_2O plot HAB and HMB compositions form sequences sub-parallel to the boundaries of the basalt types and they cut across the general trend linking all historical eruptions (see Fig.1a). On SiO_2-K_2O and P_2O_5-K_2O diagrams (Fig.1a and Fig.1b) compositions of melt inclusions in magnesian olivines (described below) are enriched with potassium over the general trends. These inclusions were not re-equilibrated and glass compositions are more evolved than bulk basalts due to post-entrainment crystallization following fractional crystallization. Based on the contrasting characteristics of HMB and HAB, Flerov et al. (1984) suggested that they have independent magma sources.

Pressure-temperature-fluid conditions in the source regions for magma generation can be estimated by inspecting the most primitive HMBs , which locally carry pyrope rich garnets, chrome-diopside presumably of mantle origin (Flerov et al., 1984). In this work we study lava of the recent 2012-2013 eruption sampled near the northern fissure (Menyailov vent area; Belousov

et al., 2015) with coordinates (55°45'47" N, 160°19'02" E). Upslope from this place (55°47'27" N, 160°20'10" E) a volcanic bomb from the 1941 eruption was sampled to get insight in the mantle source region of the Tolbachik magma with specific reference to the fluid regime.

Methods. Analyses of textures and phase compositions were performed using a CamScan MV2300 (Tescan Vega TS5130MM) SEM with an energy-dispersive spectrometer (INCA Energy 450) at the Institute of Experimental Mineralogy, Chernogolovka. The spectrometer was equipped with semi-conductive Si(Li) detector INCA PentaFET X3. Although all the phases were analyzed at an accelerating voltage of 20 kV, the current of the absorbed electrons on the optimization Co sample was 0.1-0.2 nA. Scanning area had variable shape and size for aggregates and glasses and the smallest beam diameter was 2 μm for point phase analysis. Results of measurements were processed with software package INCA Energy 200 with recalculation to weight percent concentrations using software developed by Nekrasov A.N. in IEM RAS. Water contents were determined by means of the coulometric titration on the KFT device AQUA 40.40 supplied with furnace operating at temperatures up to 1300^{o}C. Mossbauer (nuclear gamma-resonance spectroscopy) studies of the iron oxidation state of Tolbachik lavas were performed on the spectrometer MC-1104 EM (made in Rostov on Done, Russia) with ^{57}Co source in the Rh matrix.

Aerosols. A large volume of information on the syn-eruptive high temperature volcanic gases and aerosols was acquired by one of the authors (M. Zelensky) during 2012-2013 Tolbachik eruption that will be published elsewhere. Here we present only analyses of native metals in aerosols that are important in the context of understanding the generation of potassic magmas like those erupted at Tolbachik during 2012-13.

Aerosols were sampled by filtering of the volcanic gases collected in the immediate proximity from the magma flow (description of the probing site location) by using a technique described in Zelensky et al. (2013). Filters with captured particles were studied using the SEM in IEM RAS. In Fig.2a particle of the native Ni decorated with NiF_2 and Na_2SiF_6 is shown. The particle has a shape of an irregular thin plate with relatively large perimeter of c.a. 20x10 μm. Native iron (Fig.2b) was found in association with carbon and $CaCO_3$; it forms a tiny sphere with diameter of 1-2 μm. We also found an Ag ellipsoid particle containing 20% Pt with a large axis dimension of 20 μm (Fig.2c). Only iron sphere seems to be formed at the shallow magma degassing prior to eruption based on thermodynamic arguments below. Taking into account relative abundances of Fe, Ni, Ag and Pt , we suggest that native Ni and Ag+Pt were formed not from the ambient volcanic gas but from a fluid enriched with these elements and injected during magma ascent at the greater depths.

Samples from 2012-13 eruption. Two samples of the lava collected in the site near the Menyailov vents were analyzed.. Both samples contain plagioclase microlites, magnetite and rare olivine crystals. Larger laths of plagioclase are oriented parallel to flow while smaller ones have stochastic orientations. A second sample contain about 40 vol.% of vesicles. Groundmass olivine has quite uniform compositions of $Fo_{69\pm1}$ and plagioclase one is in the range An_{57-69}. Net water content in these samples was determined with the KFT method and is 0.2 and 0.26 wt.%. Sample compositions were estimated based on the phase proportions found via SEM image analysis and mean phase microprobe compositions. They appear to be in the range of the 1σ variation of those reported in Volynets et al. (2013) (see Table 1 and Fig.1). Oxidation state of iron in two lava samples was determined with Mossbauer method. Our estimate of the Fe^{3+}/Fe_{total} = 0.25-0.27 is close to the most probable ratio determined from daily statistics on Fe^{3+}/Fe_{total} ratio found with the wet chemistry analysis of GFTE-1975 lavas (supplementary materials, GFTE). Systematic observations of GFTE 1975 episodes with oxidized compositions (Fe^{3+}/Fe_{total} = 0.5) were recorded (see Fig. 3). The most reduced lavas of GFTE are characterized by Fe^{3+}/Fe_{total} = 0.2.

Deep magma conditions. It is likely that the eruption of 2012-2013 was caused by the invasion of the primitive HMB presumably with free deep fluids into the zone where evolved HAB was residing. To characterize the HMB component we analyzed olivine and Cpx phenocrysts from a bomb of 1941 eruption collected near the centre of the 2012-13 eruption. Bulk composition of the probed bomb is intermediate between highly magnesium basalts of the North and Southern breakthroughs GFTE 1975 (see Fig. 1) and much more primitive than HAB of 2012-2013 eruption. Olivine and clinopyroxene phenocrysts were extracted from the crashed samples by separation with dense liquid. In total we inspected optically about 250 grains and studied the compositions of 20 selected ones.

Olivines

The most magnesian olivine we observe was Fo_{92}. The frequency of the occurrence of the magnesian olivines (Fig.4) is distorted relative natural one and reflects our interests in this study. All olivines contain CaO in the range 0.1-0.4 wt.% which is consistent with a magmatic origin and excludes presence of mantle xenocrysts.

The most fayalitic olivines Fo_{72} have features of the dissolution and later overgrowth with Fo_{80-82} (Fig.5). The dissolution front was uneven with the formation of numerous embayments frequently closing to form fluid and melt inclusions. The most magnesian olivines have normal zoning with rims approaching Fo_{81-83} composition close to the second maximum in the histogram

(Fig.4). A single grain of magnesian olivine has a multiphase inclusion containing Cr-spinel (42.5 wt.% of Cr_2O_3), Ca-garnets with diameter of c.a. 7-10 μm (Table 2) and glass with trachyandesitic composition (Na_2O+K_2O=10.4 wt.%, SiO_2=58.3 wt.%) (see Fig. 6). This garnet contains an appreciable amount of TiO_2 (3.8 wt.%) and is close to the solid solution Andradite-Grossular-Pyrope with a high proportion of Ti-Garnet $Ca_3Mg_{0.5}AlTi_{1.5}Si_2O_{12}$ ($And_{0.25}Grs_{0.27}Py_{0.30}$Ti-$Gar_{0.14}Alm_{0.04}$). High Pyrope content indicates the high pressure of crystallization, while high Grossular is typical for alkaline magmatic garnets. Presumably the garnet bearing inclusion contains a carbonate phase with high potassium content and a low sum of cations (about 55%) on a conventional oxides basis (without CO_2) and a large fluid bubble.

A normal positive correlation of nickel concentration with magnesium content is observed in olivine phenocrysts. Overall Ni content is high and close to the compositions of Hawaiian olivines (Sobolev et al., 2005). Some points are away from the main field demonstrating unusually high Ni content for the low magnesian compositions around Fo_{72} (see Fig.7). Similar deviation from the main trend the compositional range Fo_{80-83} with NiO=0.3-0.4 wt.% was observed in phenocrysts in olivines from picrites of the Gudchikhinskaya suite underlying great PGE-Ni ore field, Norilsk area (Sobolev et al., 2009). Such enrichment in Ni of an evolved magma can be explained by its flushing with reduced carbonic fluid since as it will be shown below in this environment Ni can be a highly volatile element. In a similar way a large spread of Ni contents in Hawaiian olivines established Sobolev et al. (2005) can be explained with carbonic fluid flushing with volatile Ni redistribution within a column of rising magma or at its storage site.

Clinopyroxenes.

Clinopyroxene is present as micro-phenocrysts (~ 1 mm),, groundmass laths (~ n·10 μm) and micro-phases in the glass inclusions. Initial magnesian numbers ($Mg/Mg+Fe_{total}$) of the Cpx micro-phenocrysts is in the range of 72-78. These low magnesian Cpx crystals were not in equilibrium with magma transporting them (Fig.8a). They had experienced dissolution, reaction with the melt invading along micro-fissures (Fig.8b) and replacement or overgrowth with more magnesian Cpx (#Mg=80.5-86). One grain of Cpx with an intermediate composition (#Mg=78.3-80.5) has no signs of the interaction with the melt. In another the reaction front between Cpx and melt is propagating along a fissure with formation of the spinel (Fig. 8b). Inspection of the re-equilibration zone with microprobe demonstrates that in the reaction zone the oxidation state of iron decreases from Fe^{3+}/Fe_{total}=0.37-0.5 to 0.22-0.25 while MgO# rises from 0.73-0.75 to 0.83-0.84. However, clinopyroxenes with reduced iron and low magnesian number also exist (see Table 2). The melt filling fissure in the reaction zone is enriched in P_2O_5=0.71-1.02 wt.%,

K_2O=3.16-2.05 wt.% and TiO_2 = 2.04-2.38 wt.% at SiO_2=59-63 wt.%. The equilibrium Cpx phenocryst along with microcrystals from the glass inclusion in the chrome-spinel have the highest chromium content (0.59-0.58 wt.% Cr_2O_3 with corresponding 3-5 wt.% of Al_2O_3). These crystals are close to the composition of chrome-diopside. In some of the least magnesian Cpx crystals the sum of Al and Si cations is 1.945, which is statistically significantly less than 2 apfu and implies presence of Fe^{3+} in the tetrahedral coordination.

Melt inclusion data. The composition of the magma from the recent Tolbachik eruption was reported in (Volynets et al., 2013). Nickel content is relatively low (~25 ppm). So, in order to gain better insight into the evolution of more primitive Tolbachik magmas we analyzed melt inclusions in the olivine and clinopyroxene phenocrysts from 1941 eruption by means of EMPA. Since we did not homogenize or correct glass compositions for post-entrainment fractional crystallization and other modifications, the studied glasses appear to be more evolved (see Table 2) than bulk rock compositions reported in Volynets et al. (2013) and show larger dispersion. Mean values and 1 σ in wt.% (with bulk rock parameters in brackets) are: SiO_2 56.7±3.3 (52.3 ±1.3), TiO_2 1.55 ±0.83 (1.9±1.1), Al_2O_3 18.5±4.4 (16.1±0.3), MgO 1.7±1.0 (3.8±0.4), CaO 8.3±3.3 (7.2±0.3), FeO 4.3±2.0 (10.4±1.2), Na_2O 4.2±0.9 (3.6±0.2), K_2O 2.7±1.2 (2.4±0.1). There is an apparent correlation of K_2O with P_2O_5 (R = 0.63) but not with SiO_2 (R=0.4). Correlations between TiO_2 and Na_2O, K_2O and CaO do not appear to be significant. On the alkalies (Na_2O+K_2O)-CaO-TiO_2 ternary plot all compositions fall closely onto a single arc (see Fig.9d). Maximum TiO_2 content is reached at intermediate alkalinity and CaO content. This kind of distribution suggests that high TiO_2 content is not directly linked with alkalies.

Average potassium contents in MI is close to the average composition of Tolbachik lavas. However K_2O content has a highly variable semi-Gaussian frequency distribution (Fig. 9a). Sodium has semi-lognormal distribution (Fig.9b) with smaller relative variation (normalized on the mean value). The absence of a correlation and difference in the distribution type emphasizes the independent geochemical behaviour of Na and K. Relative abundances of Na_2O, K_2O and CaO in MI glasses are better correlated in the ternary diagram (Fig. 9c) where composition points are located within narrow band. A Ca-K array and "sodium shift" are evdent near the potassium end of this array.

Concentrations of the volatile (Cl, F, S) and trace elements are generally below analytical uncertainty level (1σ) of EMPA, however in some inclusions they reach high levels (SO_3 up to 0.9 wt.%, F up to 0.2 wt.%, Cl up to 0.3 wt.%; see Table 2). NiO content in some MI glasses is about 0.2 wt.% (2000 ppm), which is above 1σ levels of variation. Such content of nickel is

certainly much higher than reported for bulk rock Ni content of 10-70 ppm (Volynets et al., 2013). However, only some of the MIs have high concentrations of volatile components and Ni.

Careful examination reveals differences in the MI compositions hosted in the olivines with high and low Mg#. MIs in the most forsteritic olivines (n=8) have significantly lower mean CaO (5.6 versus 9.4 wt.%), TiO_2 (1.27 versus 1.8 wt.%) and higher K_2O (3.67 versus 2.68 wt.%) contents than in the most faylitic ones (n=13). Average silica content in both types was 54±3-4 wt.%. MIs in the unmodified Cpx phenocrysts have average compositions (n=12): CaO – 4.85±0.91, TiO_2 - 1.69±0.61, K_2O- 4.32±1.73. But average silica contents are significantly higher 60.3±1.95. Direct comparison of compositions of the olivine and Cpx hosted unhomogenized MIs is not possible due to the effect of post-entrainment crystallization.

fO2. Oxygen fugacity in equilibrium with melt can be estimated on the basis of the oxidation state of iron in the melt. The most comprehensive calibration correlating melt composition and temperature can be found in (Jayasuriya et al., 2004). For Tolbachik magma this oxo-barometer translates the ratio Fe^{3+}/Fe^{total}=0.25 to fO_2 = NNO-0.4 (see Fig.3). Systematic observations on the GTFE-1975 (see Fig.3) revealed that ratio the Fe^{3+}/Fe_{total} had maximum value of 0.5 that gives $fO_2 \approx$ NNO+4. Application of the monomineral oxo-barometer (Simakin et al., 2012) to the measured clinopyroxene compositions yields the lowest boundary for fO_2 equal to NNO for the Cpx micro-phenocrysts and laths with Fe^{3+}/Fe^{t}=0.17 crystallized in the magma flow at the conditions compatible with calibration ones (1050–1100°C, pressures of 2–4 kbar). Based on the observations above, we hypothesis that oxidized clinopyroxenes with low Mg# were reduced at the interaction with HMB.

On the Th/Yb-Nb/Yb diagram all Tolbachik lavas have a typical IAB position (Fig.10), which implies significant initial water content. In the subduction related lavas initial water content positively correlates with intrinsic fO_2 (corresponding to Fe^{3+}/Fe^{total} in the magmatic glasses, Kelley and Cottrell, 2009). Water content in two lava samples measured with KFT is 0.2-0.26 wt.% (approximately two times larger if recalculated to the residual glass). The Kelley and Cottrell (2009) correlation predicts initial H_2O content corresponding to the observed fO2 around NNO in the Tolbachik magma of c.a. 3.5 wt.%±1.5. The absence of amphibole in the all studied lavas of Tolbachik is consistent with a low water content in the magma below c.a. 4 wt.%. Application of the clinopyroxene sensor of the water content in the melt (Armienti et al., 2013) for five selected pairs of the MIs and host clinopyroxenes yields water concentrations of 2.87±0.24 wt.% in agreement with above estimates.

Pressure. We estimate the highest pressure encountered in our study by means of the Cr-in-Cpx barometer (Nimis and Taylor, 2000). This barometer is calibrated for garnet peridotites at

the mantle conditions. The source of Cr-diopsides in the Tolbachik magma is unclear therefore this estimate is a tentative one. After excluding of the quenching Cpx from the MI with high Al and low Cr content we get a sequence of positively correlated concentrations of Cr and Al in Cpx. We use the composition of Cpx from a glass inclusion in chrome-spinel close to a chrome-diopside ($Wo_{43.8}En_{45.2}Fs_{11.3}$) with maximum 0.59 wt.% Cr_2O_3 that yields pressure in the range 2.7-3.0 GPa at T=1100-1200^{o}C respectively (surface magma temperature was 1080^{o}C (Belousov et al., 2015 and Edwards et al., 2015)). An altered Cpx phenocryst with Cr_2O_3=0.57 (see Table 2) yields practically the same pressure range. The occurrence of melanitic andradite-grossular garnet with high pyrope content as an inclusion in olivine also indicates high pressure close to the expected magma generation level. Disequilibrium features of the mantle clinopyroxenes with low Mg# (and probably fayalitic olivines) argue for the involvement in the eruption of a deep magma ascending depths of more than 80 km. Magma ascent was sufficiently fast that disequilibrium features survived.. The position of an intermediate chamber can be estimated based on clinopyroxene –melt equilibrium predictor (Armienti et al., 2013). Five pairs of the selected MIs –Cpx compositions give P = 0.47±0.13 GPa. This estimate fits relatively well with the reconstructed depth of 17-22 km of the main magma storage zone under Tolbachik based on the geophysical data (Belousov et al., 2015).

Thermodynamic calculations.

Properties of dry carbonic fluids at high PT conditions have not been studied as well as hydrous ones. Thermodynamic analysis predicts that the stability of the mutual compounds of sulphur and carbon (COS and CS_2) will become the important components of such fluid (Simakin, 2014a). Below we show that the thermodynamic stability of the carbonyls of metals and COF_2 can explain the ability of the Tolbachik fluid to transport relatively high concentrations of Ni and we present a possible mechanism for coupled carbon and fluorine degassing.

CO in the fluid. Elemental carbon was found in Tolbachik volcanic aerosol implying at least local (around C particles) CCO buffering. Parameters of CCO buffer were calculated with thermodynamic data from (Simakin, 2014a). The highest proportion of CO in carbonic fluid is constrained by the disproportionation reaction:

$$2CO = C+CO_2, \quad (1a)$$

while oxygen fugacity is constrained by reaction

$$CO+1/2O_2=CO_2 \quad (1b).$$

It is evident that increasing pressure stabilizes CO_2 while temperature shifts endothermic CCO reaction (1b) to the left. The calculated concentration of CO at low pressures and magmatic

temperatures approaches unity and oxygen fugacity drops below IW buffer in agreement with Iacono-Marziano et al. (2012). Thus, in the presence of elemental carbon, native iron (and more electronegative elements) can form during magma degassing at low pressure (at the last several hundreds meters of magma ascent in the conduit). Our observation confirms this conclusion. However, the diameter of the observed native iron sphere (Fig.2b) is only 2 μm, which implies that during fast ascent only that a small volume of the iron was reduced in spite of the relatively large availability of this element in comparison with ppb level of Pt concentrations.

Thermodynamic modelling predicts a CO mole fraction no less than 0.1-0.2 persists even at the pressures up to 1 GPa and high T. The presence of carbon monoxide in the reduced carbonic fluid engenders a problem of the metals carbonyl stability as their potential transport form. Oxygen fugacity of Tolbachik lava during the 2012-2013 eruption was close to NNO , which corroborates our thermodynamic analysis of Ni carbonyl ($Ni(CO)_4$) stability at high PT conditions. Thermodynamic properties of $Ni(CO)_4$ and for other constituents of reaction (2) are from NIST (http://webbook.nist.gov/chemistry/). We calculate value of equilibrium constant for the carbonyl formation reaction at a wide range of PT parameters

$$Ni+4CO = Ni(CO)_4 \qquad (2)$$

When the equilibrium constant is much less than unity carbonyl is unstable at any concentration of CO. For K>>1 it will form even at small concentrations of CO. Tentatively we set the stability boundary within area of $5<\log(K)<-1$. Obviously this transition is strongly stabilized by pressure. At the ambient pressure nickel carbonyl is decomposed when heated above above 80-130^{o}C. For industrial production of fine Ni powder pressure drop induced carbonyl decomposition is used. These properties of Ni(CO)4 are in agreement with our calculations. At elevated pressures fugacity coefficients of the carbonyls are not known, therefore we set some reasonable fugacity coefficients and assume ideal mixing of the non-ideal components. Although our stability analysis is preliminary and needs experimental verification, we find that at upper crustal pressures (P=0.3 GPa) it is expected to be stable at temperature less than approximately 670^{o}C. At 1GPa the stability temperature of $Ni(CO)_4$ is approaching magmatic ones of around 1000^{o}C (see Fig.11a). At the same time in accordance with thermodynamic modelling iron pentacarbonyl appears to be unstable even at 1 GPa at magmatic temperatures (see Fig.11b). This estimate contradicts that suggested by Wetzel et al. (2013) for CO dissolution in ultrabasic melt at P=1 GPa and T=1300^{o}C as $Fe(CO)_5$. Probably the more stable poly-nuclear iron carbonyl is involved in the CO dissolution reported in the Wetzel et al. (2013) experiments.

Dry carbonic fluid can extract fluorine from the magmatic melt. This condition is consistent with our observation that in Tolbachik aerosols (see Fig.2a) native Nickel is decorated with NiF_2 and at high PT conditions this compound is present in the fluid. We suggest that one of the

possible mechanisms of fluorine degassing is linked with NiF_2 reduction to metalic nickel by carbon monoxide with its extraction from the melt:

$$NiF_2(g) + CO(g) = Ni(s) + COF_2\ (g) \qquad (3)$$

We calculated the equilibrium constant of reaction (3) using thermodynamic properties of the gaseous NiF_2 taken from (http://www.chem.msu.su/Zn/Ni). This reaction is characterized by ΔG_r = -130.3 kJ due to a quite large ΔG_f of COF_2 and negative ΔS_r (- 171 J/mol/K). With increasing T this reaction is shifted to the left ($\Delta S_r<0$) while pressure stabilizes native Ni production (see Fig.12). More electronegative metals (with higher tendency to the native state such as Ag, PGE) will make fluorine extraction by means of the reaction (2) more efficient. COF_2 is synthesized by the reaction $2AgF+CO=2Ag+COF_2$. COF_2 is stable only in the dry fluid and is strongly subject to hydrolysis (Wofsy et al., 1990)

$$COF_2 + H_2O = CO_2 + 2HF \qquad (4)$$

HF produced in this reaction may react back with the melt and locally enrich it with fluorine. Certainly other compounds such as mixed carbonates and fluorides are suitable candidates for the fluorine extraction from the silicate melt. It is important to note that during 1975 Tolbachik eruption the flux of gaseous F was high and various fluorine salts were abundant in the high temperature exhalations (Braitseva et al., 1984).

Discussion.

The origin of ultra-potassic low silica magmas is confidently linked with melting of the fertile mantle in the presence of a CO_2 dominated fluid (Gupta, 2015). Indeed mantle fertilization (metasomatism) and partial melting can be two sides of the same process induced by production of carbonic fluid by decarbonatization reactions and mantle pyroxenization. Recycled crustal material is accepted as a source of carbon for these processes (Gupta, 2015). Obviously the potassic trend in Tolbachik lavas is only weakly expressed if compared with true ultrapotassic rocks. However, rare occurrences such as melilite xenoliths (Flerov et al., 1984), melanitic garnet and chrome-diopsides (see above) can be explained by the existence of the potassic alkaline melts in the mantle at the depths 60-80 km (P=2-2.5 GPa) under Tolbachik. Typical mineralogy of ultrapotassic magmas includes these phases (Gupta, 2015).

Berkesi et al. (2012) show that carbonic fluid at 1-1.5 GPa transported Na_2O, Al_2O_3, MREE and Ti by comparing mantle xenoliths rich- and poor in CO_2 micro-fluid inclusions ,enriching host clinopyroxenes with these components. A similar conclusion on the appreciable solubility of Al_2O_3 in a reduced carbonic fluid with low water content at P=0.3-0.5 GPa and T= 500-600^oC was made based on the study of the fluid inclusions in the rubies from marbles with organic carbon (Giuliani et al., 2003). In accordance with our experimental data (Simakin et al., 2015)

dry reduced carbonic fluid is a good solvent and carrier for LREE, alkalies and Al_2O_3 even at low pressure 0.2-0.5 GPa and T=900-1000^oC. Moreover in our experiments dry reduced carbonic fluid generated peralkaline potassic melt on the Ol-Spl matrix by extraction and deposition of alumo-silicates from the basaltic melt. Our results support conclusions of Kaszuba and Wendlandt (2000) that the formation of alkaline potassic partial melt from alkaline basalt at P = 0.7 -1.0 GPa is facilitated by a high ratio $CO_2/(H_2O+CO_2)$=0.9 in the fluid. The presence of fluorine in such a carbonic fluid (see above) would enhance the mobility of HFSE. For example in the potassic lavas of Lewotollo (Indonesia), ziconolite decorates vesicle walls (de Hoog and van Bergen, 2000). The observed HFSE transport is explained by the high fluorine content in the fluid. Thus one can expect a correlation among the concentrations of K_2O, LREE and HFSE in Tolbachik magmas if flushing by a reduced carbonic fluid through the magma or during mantle metasomatism happened.

K_2O-trace elements correlations. Our experimental data (Simakin et al., 2015) argues for an especially high LREE mobility in carbonic fluid. Indeed a strong correlation of K_2O and Ce (LREE) concentrations is observed for Alicudi volcano (Aeolian arc, (Peccerillo et al., 2013)), volcanoes Kamen (KGV, (Churikova et al.,2013)), Tolbachik (Volynets et al., 2013) and Sedanka volcanic center (Volynets et al., 2010) (Fig.13a). Behavior of HFSE is dictated by fluorine and indirectly by CO_2. (see Fig.13a). Strong correlation of Zr and K_2O concentrations in lavas of various volcanoes is encountered (Fig. 13b). In the whole considered Kamchatka volcanoes demonstrate high Zr concentrations in lavas at the similar potassium contents significantly above Lewotollo volcano lavas, where Zr is mobile in the fluid. Both fluid addition and fractional crystallization may have similar expression for the chosen incompatible elements. To evaluate scale of fractional crystallization effect we use expression for the normalized on the initial value (C_0) concentration C_{fract} of the trace element in magma: $C_{fract}/C_0 = \alpha_m^{K_D-1}$, here K_D is generalized distribution coefficient solid/melt and α_m is fraction of the unsolidified magma. It is evident that at K_D=1 there is no fractionation and concentration is constant. At K_D=0 maximum effect of the trace element fractionation has place. In fact K_D is effective coefficient including effect of the interstitial melt accumulation at the crystal settling and its value depends on the dynamics of the compaction of the crystal mush. In the Figure 13 we plot ranges of the α_m providing observed concentration rise for particular element (K_2O or Ce, Zr) while using K_D in the range 0-0.2. To cause co-variations of K_2O, Zr and Ce for lava compositions from (Churikova et al., 2013) it is enough to crystallize approximately one half of the magma. While excluding extreme variations of compositions of lavas from Sedanka both on the K_2O-Ce and K_2O-Zr diagrams are well within ranges of the fractional crystallization effect of approximately

one half of magma too (0.6-0.33). Not all variations within groups are accurately explained at such simplified approach there are large deviations from the linear trends on concentration diagrams that can be linked with specific effects of fractional crystallization or fluid addition. Transfer from one group to another can be attributed to the change of the source of magma, e.g. due to mantle fertilization by deep fluid. To attribute variation in the whole concentration range (e.g. for K2O 0.75-3.5 wt.%) to fractional crystallization the separation of 0.15-0.2 of the residual melt is required. This seems to be inconsistent with the fast magma accumulation and eruption rates in the active volcanic areas.

Native metals. The composition of the observed metal particles can be compared to those whose origins have already been established.. High fugacity of hydrogen is reached at relatively low temperature during the serpentinization of olivine-rich rocks. In serpentinite, hydrogen formed by the conversion of ferrous (Fe_2SiO_4) to ferric (Fe_3O_4) iron in the presence of a hydrous fluid produces Fe-Ni alloy (Dekov, 2006). The observed Ni and Ag-Pt particles from Tolbachik aerosols are quite different from this alloy and from the native Pb-Sn, Zn-Cu alloys reportedly found in a fumarole of GFTE-1975 (Glavatskih, 1990). The later ones contain much more abundant Pt and Ni metals and their further accumulation may have been facilitated by longer interactions with fluids and with rocks. In tephra from Shiveluch native zinc was found (Karpov and Mohov, 2004). Pt-Fe alloy not Ag-Pt is typical for the upper mantle (Bai et al, 2000). At the same time Ag-Cu alloy is suggested to have mantle origin in the zone of the MORB generation (Dekov and Damyanov, 1996). We propose that in our case CO and COS in the fluid are responsible for the formation of the observed metallic particles from Tolbachik aerosols. The reduced carbonic fluid with PT parameters within the stability field of Ni carbonyl stability can be assimilated by ascending basaltic magma. A high concentration of Ni in the deep fluid can be produced by infiltration through the mafic rocks with high Ni contents. After being assimilated into the Tolbachik magma this fluid will thermally decompose with formation of the large native Ni particles, which would travel in the growing fluid bubbles up to the level of magma fragmentation and then be transferred to the aerosol phase. Another factor favouring native metals formation is reduction of the sulphur activity in the fluid due to the formation of COS in the dry fluid at high P and low fO2 (Simakin, 2014a). COS is expected to be a good solvent for PGE. Complexes such as $Pt(CO)Cl_2$ with CO may be also responsible for the concentrating of noble metals and enabling formation of the Ag-Pt alloy described above during fluid assimilation into magma. Sporadic spikes of the volatiles and Ni contents in MI support this suggestion, since fluid injected between eruptions will produce inhomogeneous magma with local composition variations around bubbles. High volume percolation through deep metamorphic rocks of the amphibolite and granulite facies by the fluid leading to the production of graphite has been

recognized in the Russian Far-East (Khanchuk et al., 2013). Graphitized rocks contain micron and submicron particles of native Au, Ag, Pt and PGE intermetalides. Khanchuk et al. (2013) argue that graphite and native metals are deposited from a reduced carbonic fluid of endogenic origin. We suggest that a similar composition of fluid was also present at depth beneath the Tolbachik system.

Assumed carbon enrichment of the mantle under KGV can be explained by the geologically recent accretion of Kronotsky paleoarc from 5 Myrs (north) to 10 Myrs (south) ago (Soloviev, 2008). In the new geodynamic model (Simakin, 2014b) once certain rheologic parameters are reached the accreted terrains are overstepped by the subduction zone causing a temporary inversion of the subduction direction. During the inversion large blocks of the accreted arc are pushed under the mantle wedge. The Krontsky paleoarc was formed at latitudes close to the equator in Cretaceous time and was enriched in organic (coal) and silicified carbonate rocks (Saveliev et al., 2007). Large masses of such rocks rise as diapirs due to their extreme density contrasts with the surrounding mantle wedge. In the subducting slab relatively low temperatures and high pressures preclude reaction of the silica and carbonates. As the diapirs are ascending within the mantle wedge they will begin to react at the intersection of the stability boundary for the decarbonatization reaction in PT space (Martin and Hammouda, 2011). CO_2 generated in the mantle will ascend and may accumulate in the lower crust. Existence of such deep reservoirs of carbon dioxide is anticipated by Frezzotti et al. (2009). We suggest that magma ascending from mantle or from the deepest storage near the Moho will intersect this layer and experience flushing by the reduced carbonic fluid.

Massive input of silicified carbonates and coal into the mantle wedge probably happened several millions years ago near the Central Ridge position in a back arc setting. By the slow circulation in the mantle wedge carbonatized zones would migrate eastward with time until it reached a position beneath the KGV and Tolbachik volcano. Pyroxenitic slab under KGV that might be the product of carbonatization reaction is suggested at a depth 100 km based on seismic and petrologic data (Nikulin et al., 2012). On the Th/Yb-Nb/Yb classification diagram (Fig. 10) Tolbachik lavas occupy the IAB field implying their formation by subduction water fluid fluxing. High Ca and Ti content in Tolbachik magmas can be attributed to the pyroxenite composition (Nikulin et al., 2012) of the parental mantle source. During ascent this magma will interact with potassic alkaline partial melts and carbonic fluid that will modify its composition. Southern part of Kronotsky paleoarc was accreted earlier and carbonatized mantle there was moved by convection in the mantle wedge towards eastern Kamchatka shore and its effect probably can be seen at Avacha volcano, where in shallow mantle xenoliths native Ni (Ishimaru

et al., 2009) and unusual metasomatic Ni enrichment of olivine grains up to 7 wt.% of NiO have been reported (Ishimaru and Arai, 2008).

Conclusions.

It is well established that crustal carbon has an important role in the generation of ultra-potassic low silica magmas such as lamproites. But its role in the formation of moderately potassic basalts like those of the KGV is not so clear. However, there are indirect signs of the involvement of a reduced carbonic fluid in their genesis. The signs include discovery of the native Ni and PGEs in the aerosols of Tolbachik 2012-2013 eruption, in addition to the occurrence of melanitic garnet as an inclusion in olivine from the 1941 Tolbachik eruption and an earlier reported melilitic xenolith in Tolbachik lava (Braitseva et al., 1984). During recent accretion of Kronotsky arc to Kamchatka large masses of the silicified carbonates and coals could be dragged under the mantle wedge and may cause subsequent mantle wedge pyroxenization affecting magma generation in the subduction zone.

Acknowledgements. This study was incredibly benefited from the cooperation with Alexey Nekrasov (EMPA, Chernogolovka, IEM RAS). We deeply appreciate constructive reviews of Pietro Armienti (Pisa University) and Andrey Girnis (IGEM RAS) and great efforts of guest editor of this issue M.Belousova, in improving English and in adding clearness to this manuscript. AS and TS thank financial support of RFBR grants (#13-05-00397 and 13-05-00994).

References.

Armienti, P., Perinelli C. and Putirka, K.D. 2013. A New Model to Estimate Deep-level Magma Ascent Rates, with Applications to Mt. Etna (Sicily, Italy). J. Petrol. 54 (4), 795-813.

Bai, W., Robinson, P.T., Fang, Q., Yang, J., Yan, B., Zhang, Z., Hu, X.-F., Zhou, M.-F. and Malpas, J., 2000. The PGE and base-metal alloys in the podiform chromitites of the Luobusa ophiolite, Southern Tibet. Canadian Mineral. 38, 585-598.

Belousov, A., Belousova, M., Edwards, B., Volynets, A., Melnikov, D., 2015. Overview of the precursors and dynamics of the 2012–13 basaltic fissure eruption of Tolbachik Volcano, Kamchatka, Russia. J.Volcanol. Geotherm. Res. (in press).

Berkesi, M., Guzmics, T., Szabo, C., Dubessy, J., Bodnar, R.J., Hidas, K., Ratter, K., 2012. The role of CO2 rich fluids in trace element transport and metasomatism in the lithospheric mantle beneath the Central Pannonian Basin, Hungary, based on fluid inclusions in mantle xenoliths. Earth Planet. Sci. Lett. 331–332, 8–20.

Braitseva, O.A., Melekestsev, I.V., Flerov, G.V., Ponamarev, V.V., Sulerzhitskii, L.D., Litasova S.N., 1984. Holocene magmatism of the Tolbachik regional zone of the cinder cones. In: Fedotov, S.A., (Ed.), Great Fissure Eruption of Tolbachik. Nauka, Moscow, pp.177-209 (in Russian).

Churikova, T.G., Gordeychik, B.N., Ivanov, B.V., Wörner, G., 2013. Relationship between Kamen Volcano and the Klyuchevskaya group of volcanoes (Kamchatka). Journal of Volcanology and Geothermal Research 263, 3-21.

Conticelli, S., Boari, E., Avanzinelli, R., De Benedetti, A.A., Giordano, ZG., Mattei, M., Melluso, L., Morra, V., 2010 Geochemistry, isotopic composition and petrogenetic modelling of the Colli Albani volcanic rocks. In: Funiciello, R., Giordano, G. (Eds.), The Colli Albani Volcano. Special Publications of IAVCEI, The Geological Society, London, UK, 3, pp.107–139.

Cortes, J., Wilson, M., Condliffe, E., Francalanci, L., 2006. The Occurrence of Forsterite and Highly Oxidizing Conditions in Basaltic Lavas from Stromboli Volcano, Italy. J. Petrol. 47, 1345–1373.

Dekov V., 2006. Native nickel in the TAG hydrothermal field sediments (Mid-Atlantic Ridge, 26^{o}N): Space trotter, guest from mantle, or a widespread mineral, connected with serpentinization? J Geophys. Res. 111, B05103, doi:10.1029/2005JB003955.

Dekov, V.M. and Damyanov, Z.K., 1997. Native silver-copper alloy in metalliferous sediments from the East Pacifie Rise axial zone (20° 30'-22° 10'S). Oceanologica Acta. 20(3), 501-512.

Edwards, B.R., Belousov, A., Belousova, M., Melnikov, D., 2015. Observations on lava, snowpack and lava–snowpack interactions during the 2012–13 Tolbachik eruption, Klyuchevskoy Group of Volcanoes, Kamchatka, Russia. J. Volcanol. Geotherm. Res. (in press).

Flerov, G.B., Andreev, V.N., Budnikov, V.A., Ponamarev, V.V., Tsyurupa, A.I., 1984. Petrology of the eruption products. In: Fedotov, S.A., (Ed.), Great Fissure Eruption of Tolbachik. Nauka, Moscow, pp.223-276 (in Russian).

Frezzotti, M.L., Peccerillo, A., Panza, G., 2009. Carbonate metasomatism and CO2 lithosphere-astenosphere degassing beneath the western mediterranean: an integrated model arising from petrological and geophysical data. Chemical Geol. 262, 108–120.

Giuliani, G., Dubessy, J., Banks, D., 2003. CO_2–H_2S–COS–S_8–AlO(OH) bearing fluid inclusions in ruby from marble hosted deposits in Luc Yen area, North Vietnam. Chem. Geology. 194. 167–185.

Glavatskih, S.F., 1990. Native metals and intermetalic compounds in products of exhalations of GFTE (Kamchatka). Doklady Earth Sciences. 313(2). 434-437.

Glavatskikh, S.F., Trubkin, N.V., 2000. First findings of native tungsten and silver in exhalation products of the Tolbachik Great Fissure Eruption, Kamchatka. Doklady Earth Sciences. 373a, 997-999.

Gordeev, E.I., Karpov, G.A., Anikin, L.P., Krivovichev, S.V., Filatov, S.K., Antonov, A.V., Ovsyannikov, A.A., 2014. Diamonds in the lavas of fissure Tolbachik eruption in Kamchatka. Doklady Earth Sciences 454, part2, 204–206.

Grebennikov, A.V., Shcheka, S.A., and Karabtsov, A.A., 2012. Silicate–metallic spherules and the problem of the ignimbrite eruption mechanism: the Yakutinskaya volcanic depression. J. Volcanol. and Seismol. 6(4), 211–229.

Gupta, A.K., 2015. Origin of Potassium-rich Silica-deficient Igneous Rocks. Springer, India.

de Hoog, J.C.M., 2001. Behavior of volatiles in arc volcanism Geochemical and petrological evidence from active volcanoes in Indonesia. Ph.D. Dissertation, Utrecht University, Netherlands.

de Hoog, J.C.M., van Bergen, M.J., 2000. Volatile induced transport of HFSE, REE, Th and U in arc magmas: evidence from zirconolite-bearing vesicles in potassic lavas of Lewotollo volcano (Indonesia). Contrib. Mineral. Petrol. 139, 485-502.

Iacono-Marziano, G., Gaillard, F., Scaillet, B., Polozov, A.G., Marecal, V., Pirre, M., Arndt, N.T., 2012. Extremely reducing conditions reached during basaltic intrusion in organic matter-bearing sediments. Earth Planet. Sci. Lett. 357-358, 319-326. DOI : 10.1016/j.epsl.2012.09.052.

Ishimaru, S., Arai, S., 2008. Nickel enrichment in mantle olivine beneath a volcanic front Contrib. Mineral. Petrol. 156, 119–131.

Ishimaru, S., Arai, S., Shukuno, H., 2009. Metal-saturated peridotite in the mantle wedge inferred from metal-bearing peridotite xenoliths from Avacha volcano, Kamchatka. Earth Planet. Sci. Lett. 284, 352–360.

Jayasuriya, K.D., O'Neill, H.St.C., Berry, A.J., Campbell, S.J., 2004. A Messbauer Study of the Oxidation State of Fe in Silicate Melts. Am. Mineral. 89, 1597–1609.

Karpov, G.A. and Mokhov, A.V., 2004. Accessory Native Ore Minerals in Eruptive Ashes Discharged by Andesitic Volcanoes of Kamchatka. Volcanol. Seismol., 4, 41-49.

Kaszuba, J.P., Wendlandt, R.F., 2000. Effect of carbon dioxide on dehydration melting reactions and melt compositions in the lower crust and the origin of alkaline rocks. J. Petrol, 41(3), 363-386.

Kelley, K.A., Cottrell, E., 2009. Water and the oxidation state of subduction zone magmas. Science, 32, 605-607.

Khanchuk, A.I., Plyusnina, L.P., Ruslan, A.V., Likhoidov, G.G. and Barinov, N.N., 2013. Nature of Graphitization and Noble Metal Mineralization in Metamorphic Rocks of the Northern Khanka Terrane, Primorye. Geology of Ore Deposits. 55(4), 225–244.

Lukanin, O.A., Kadik, A.A., Biggar, G.M., Fedotov, S.A., 1980. Physico-chemical conditions of tcrystallization of Tolbachik Great Fissure Eruption 1975-1976 basalts. Volcanol. Seismol., 3, 16-50.

Martin, A.M., Hammouda, T., 2011. Role of iron and reducing conditions on the stability of dolomite + coesite between 4.25 and 6 GPa – a potential mechanism for diamond formation during subduction. Eur. J. Mineral. 23, 5–16.

Nikulin, A., Levin, V. , Carr, M. , Herzberg, C. , West, M., 2012. Evidence for two upper mantle sources driving volcanism in Central Kamchatka. Earth Planet. Sci. Lett. 321-322, 14–19.

Nikogosian, I.K., van Bergen, M.J., Manfred, J., 2010. Heterogeneous mantle sources of potassium-rich magmas in central-southern Italy: Melt inclusion evidence from Roccamonfina and Ernici (Mid Latina Valley). Journal of Volcanology and Geothermal Research 197(1), 279-302.

Nimis, P., Taylor, W., 2000. Single clinopyrxene thermobarometry for garnet peridotites. Part I. Calibration and testing of Cr-in-Cpx barometer and enstatite-in Cpx thermometer. Contrib. Mineral. Petrol. 139, 541-554.

Pearce, J.A., Peate, D.W., 1995. Tectonic implications of the composition of volcanic arc magmas. Annual Review of Earth and Planetary Sciences 23, 251-285.

Peccerillo, A., De Astis, G., Faraone, D., Forni, F., Frezzotti, M. L., 2013. Compositional variations of magmas in the Aeolian arc: implications for petrogenesis and geodynamics.
In: Lucchi,F., Peccerillo, A., Keller, J. , Tranne,C.A., Rossi,P. L., (Eds.), The Aeolian Islands volcanoes, Geological Society, London, Memoirs 37, chapter15, pp491-510.

Ponamareva, V., Portnyagin, M., Derkachev, A., Pendea, I. F., Bourgeois, J., Reimer, P.J., Garbe-Schonberg, D., Krasheninnikov, S., Nurnberg, D., 2013. Early Holocene M~6 explosive eruption from Plosky volcanic massif (Kamchatka) and its tephra as a link between terrestrial and marine paleoenvironmental records. International Journal of Earth Sciences 102 (6), 1673-1699.

Saveliev, D.P., Lander, A.V., Pronina, N.V., Savelieva, O.L., 2007. First finding of the coal rocks in the Cretaceous paleo-oceanic complexes of Eastern Kamchatka. Vestnik KRAUNZ Earth sciences 2(10), 102-104 (in Russian).

Seliverstov, N.I., 2007. Structure of the seismofocal zone of Kamchatka. Vestnik KRAUNZ Earth sciences 1(9), 10-26 (in Russian).

Simakin, A.G., Devyatova, V.N., Salova, T.P., Zelensky, M.E., 2015. On the role of the essentially CO_2 fluid in the origin of the magmas and magmatic ores. Doklady Earth Sciences. (in press).

Simakin, A.G.. 2014a. Peculiarities of the fluid composition in the dry C-O-S system at PT parameters of the low crust by the data of the thermodynamic modeling. Petrology 22(1),50-59.

Simakin, A.G., 2014b. Numerical modelling of the late stage of subduction zone transference after an accretion event. Terra Nova 26(1), 22–28.

Simakin, A. G., Salova, T. P., Bondarenko, G.V., 2012. Experimental Study of Magmatic Melt Oxidation by CO2. Petrology 20(7), 593–606.

Sobolev, A.V., Sobolev, S.V., Kuzmin, D.V., Malitch, K.N., Petrunin, A.G., 2009. Siberian meimechites: origin and relation to flood basalts and kimberlites. Russian Geology and Geophysics 50, 999–1033.

Sobolev, A.V., Hofmann1, A.W., Sobolev, S.V., Nikogosian, I.K., 2005. An olivine-free mantle source of Hawaiian shield basalts. Nature 434, 590-597.

Soloviev, A.V., 2008. The study of tectonic processes in the areas of lithospheric plates convergence: methods of track dating and structural analysis. Proceedings of Institute of Geology RAS. Nauka, Moscow. (in Russian).

Supplementary materials, 1984. In: Fedotov, S.A., (Ed.), Great Fissure Eruption of Tolbachik. Nauka, Moscow, pp.177-209 (in Russian).

Teague, A.J., Hanley, J., Seward, T.M., Reutten, F., 2011. Tracy-element distribution between coexisting aqueous fumaroles condensates and natrocarbonatite lavas at Oldoinyo Lengai volcano, Tanzania In: Beccaluva, L., Bianchini, G., Wilson, B.M., (Eds.), Volcanism and Evolution of the African Lithosphere. Geol. Soc. Amer. Special Paper. 478, 159–171.

Volynets, A.O., Churikova, T.G., Worner, G., Gordeychik, B.N., Layer, P., 2010. Mafic Late Miocene–Quaternary volcanic rocks in the Kamchatka back arc region: implications for subduction geometry and slab history at the Pacific–Aleutian junction. Contrib. Mineral. Petrol. 159, 659–687. DOI 10.1007/s00410-009-0447-9.

Volynets, A. O., Melnikov, D. V., Yakushev ,A. I., 2013. First data on the composition of the products of the Tolbachik fissure eruption named by 50th anniversary of IVAS (Kamchatka). Doklady Earth Sciences 452(1), 953-957.

Volynets, A.O., Edwards, B.R., Melnikov, D.,Yakushev, A., Griboedova I., 2015. Monitoring of the volcanic rock compositions during the 2012–2013 fissure eruption at Tolbachik volcano, Kamchatka. J.Volcanol. Geotherm. Res. (in press).

Wetzel, D.T., Rutherford, M.J., Jacobsen, S.D., Hauri, E.H., Saal, A.E., 2013. Degassing of reduced carbon from planetary basalts. Proc. Natl. Acad .Sci. USA. 110(20): 8010–8013.

Wofsy, S.C., Yatteau, J.H., Salawitch, R.J., McElroy,M.B., Toon,G.C., Mankin, W.G., Coffey, M.T., 1990. Heterogeneous conversion of COF2 to HF in polar stratospheric clouds. Geophysical Research Letters 17(4), 461-464.

Zelenski, M.E., Fischer, T.P., Maarten de Moor, J., Marty, B., Zimmermann, L., Ayalewd, D., Nekrasov, A.N., Karandashev V.K., 2013. Trace elements in the gas emissions from the Erta Ale volcano, Afar, Ethiopia. Chemical Geology 357, 95–116.

Figure captions

Figure 1. Geochemical plots of data from historical eruptions of Tolbachik volcano: a) SiO_2-K_2O classification diagram, and b) P_2O_5-K_2O diagram; semi-filled diamonds are GFTE-1975 lavas of the North and South breakthroughs (from (Supplementary.., 1980), on b) averaged data), open triangle – bomb of 1941 eruption, open circles – FTE 2012 (v-average of (Volynets et al., 2015), empty –our data), filled stars stay for the averaged MIs from Fe-rich and Fo-rich olivines. On both plots melt inclusions in high magnesium olivines are characterized by the potassium content higher than in the main sequence.

Figure 2. Native metals from aerosols collected at Tolbachik eruption of 2012-2013 year.

Figure 3. Histogram of the bulk Fe^{3+}/Fe_{total} for the lavas of the initial stage of the GFTE-1975 calculated with previously published data (Supplementary.., 1980). The most probable value of ratio at the treatment with model by Jayasuriya et al. (2004) corresponds to an oxygen fugacity around NNO. Maximum observed Fe^{3+}/Fe_{total} yields rather high $fO_2 \approx$ NNO+4. Black horizontal rectangle denotes range of the ratio in two samples of FTE 2012 determined by Mossbauer method.

Figure 4. Histogram of Mg-number of olivines (forsterite mole fraction) analyzed in this study. Left rectangle shows the range of the groundmass olivine compositions of samples from the 2012-2013 Tolbachik eruption; right square is the composition of olivine with garnet in the MI.

Figure 5. Dissolution structures in olivines. a) SEM image of the partially dissolved and overgrown fayalitic Ol crystal with inverse zonality in false colors. b) Optical image of the multiphase inclusion in the healed dissolution defect, scale bar 20 μm.

Figure 6. Multiphase inclusion in magnesian olivine: 1) Cr-spinel, 2) garnet, 3) carbonate, and 4) glass. In the upper insert SEM view of the same inclusion before additional polishing, in the lower insert optic image of the garnet from the same olivine grain. Large void is decorated by tiny crystalline phases precipitated from the fluid phase. The long dimensions for the scale rectangles are: 1) 25 μm in the upper insert 2) 10 μm for the main image 3) 10 μm for the lower insert.

Figure 7. Nickel content in the studied olivines from Tolbachik; colored fields show Hawaiian olivines compositions: Koolau (green), Mauna Loa – (grey) (from Sobolev et al., 2005). Horizontal dashed line denotes 1 σ uncertainty for NiO analysis by EMPA. Dotted rectangle shows range of composition of the equilibrium compositions on the moment of mixing.

Figure 8. Clinopyroxenes from Tolbachik. a) Optical image of the reaction zone between low magnesian Cpx and melt, rectangle width is 20 μm. b) SEM image of the disequilibrium low Mg Cpx phenocryst.

Figure 9. MIs compositions. a) K_2O frequency distribution histogram. b) Na_2O frequency distribution histogram. c) Ternary plot of atomic concentrations of Na, K and Ca. d) ternary plot of atomic concentrations of Na+K, Ca and Ti.

Figure 10. Th/Yb – Nb/Yb diagram (Pearce and Peate, 1995). Samples from Tolbachik plot in the Tolbachik is IAB field and samples from Sedanka plot in the OIB field.. The Sedanka volcanic center started activity at 3-3.5 Ma in back-arc position.

Figure 11. Carbonyls stability fields contoured by isolines for K_{react} of 10^5 and 0.1. a) Pressure-temperature stability range for $Ni(CO)_4$ and for b) $Fe(CO)_5$

Figure 12. Equilibrium constant (***log(K$_r$)***) of reaction (3) at high PT conditions.

Figure 13. Correlations between K_2O and incompatible trace elements in basaltic lavas. a) Ce b) Zr. On the plot we show residual melt fractions required to cause indicated by the arrows variations of melt composition at the fractional crystallization. The distribution coefficient K_D was in the range 0-0.2.

Figure 1

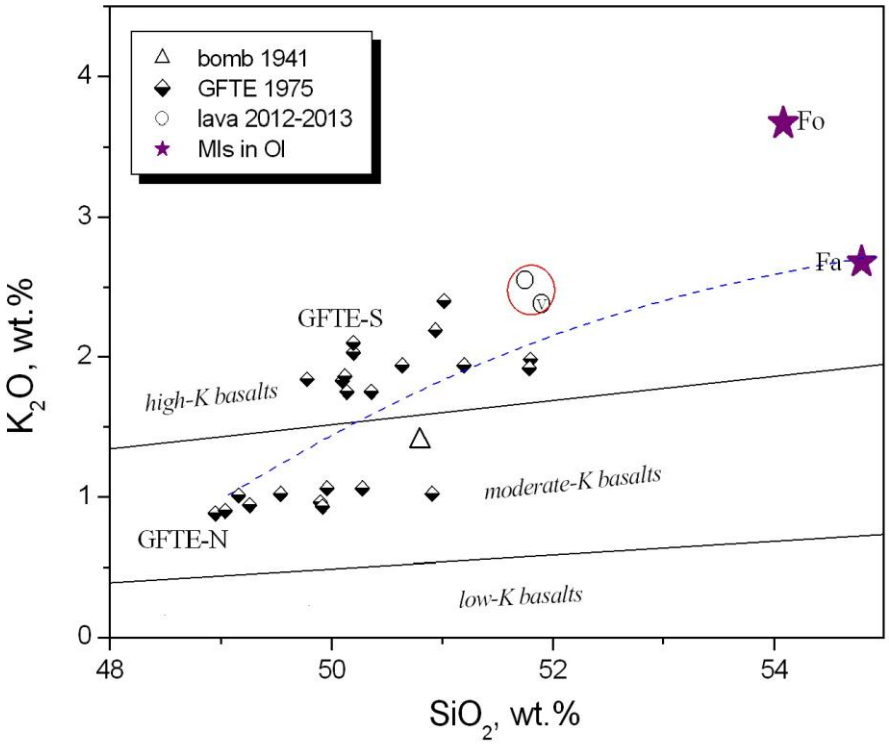
bomb 1941
GFTE 1975
lava 2012-2013
MIs in Ol
Fo
Fa
GFTE-S
high-K basalts
moderate-K basalts
GFTE-N
low-K basalts
K2O, wt.%
SiO2, wt.%
0
1
2
3
4
48
50
52
54

A

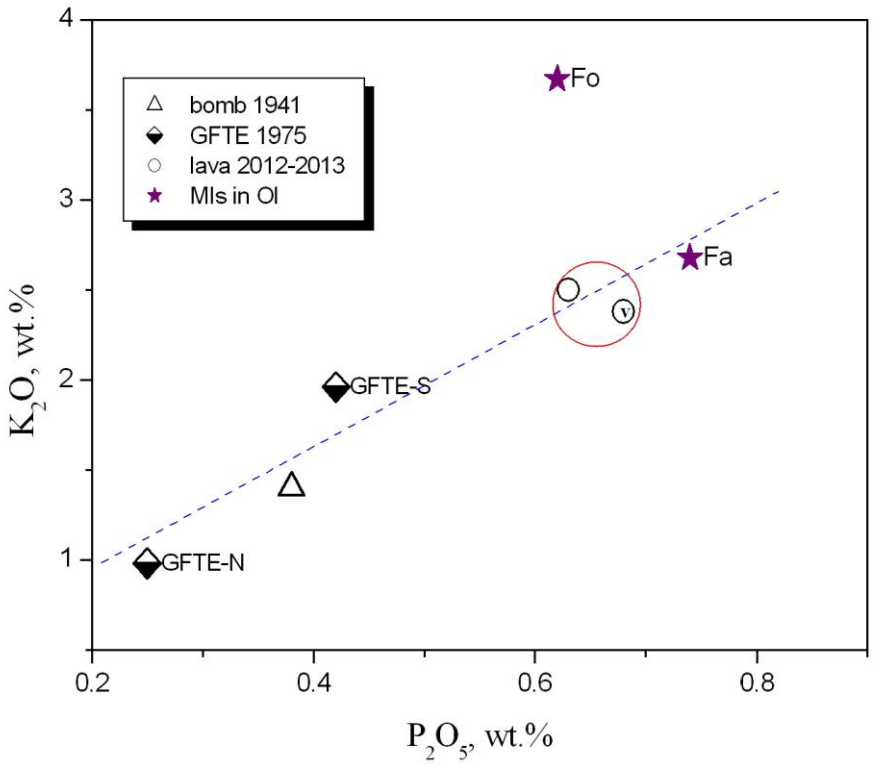
bomb 1941
GFTE 1975
lava 2012-2013
MIs in Ol
Fo
Fa
GFTE-S
GFTE-N
K2O, wt.%
P2O5, wt.%
1
2
3
4
0.2
0.4
0.6
0.8

B

Figure 2

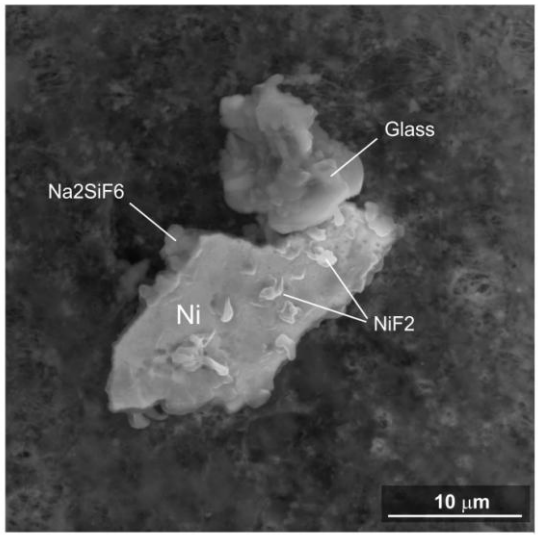

A

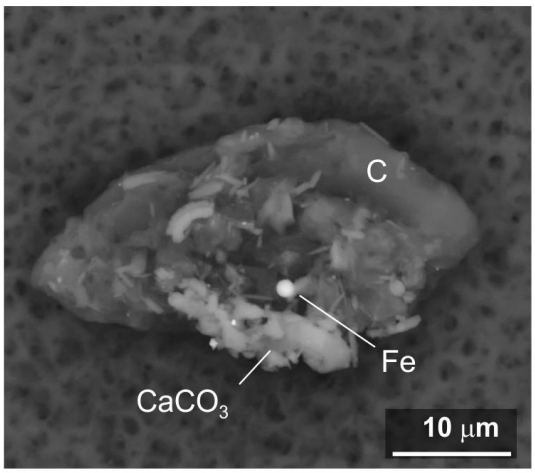

An aggregate of carbon, calcite native iron

B

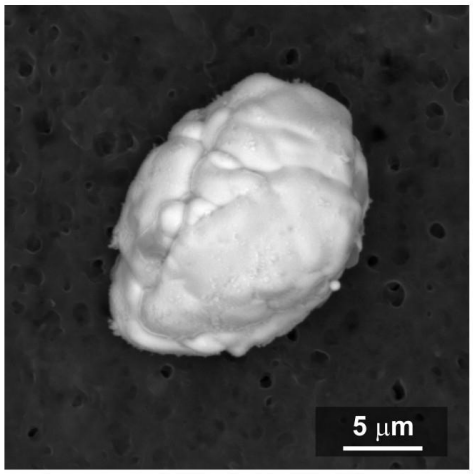

Ag 80%, Pt 20% (wt.)

C

Figure 3

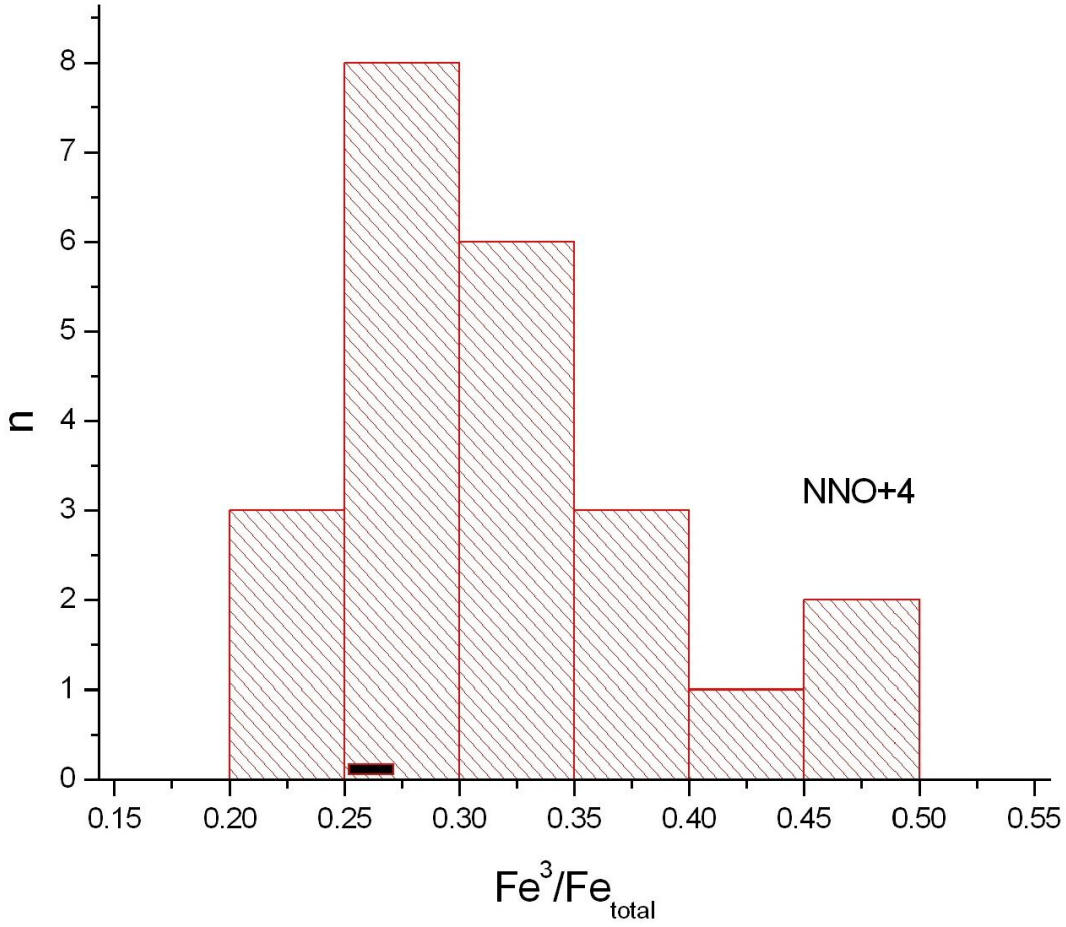
n
0
1
2
3
4
5
6
7
8
0.15
0.20
0.25
0.30
0.35
0.40
0.45
0.50
0.55
NNO+4
Fe3/Fetotal

Figure 4

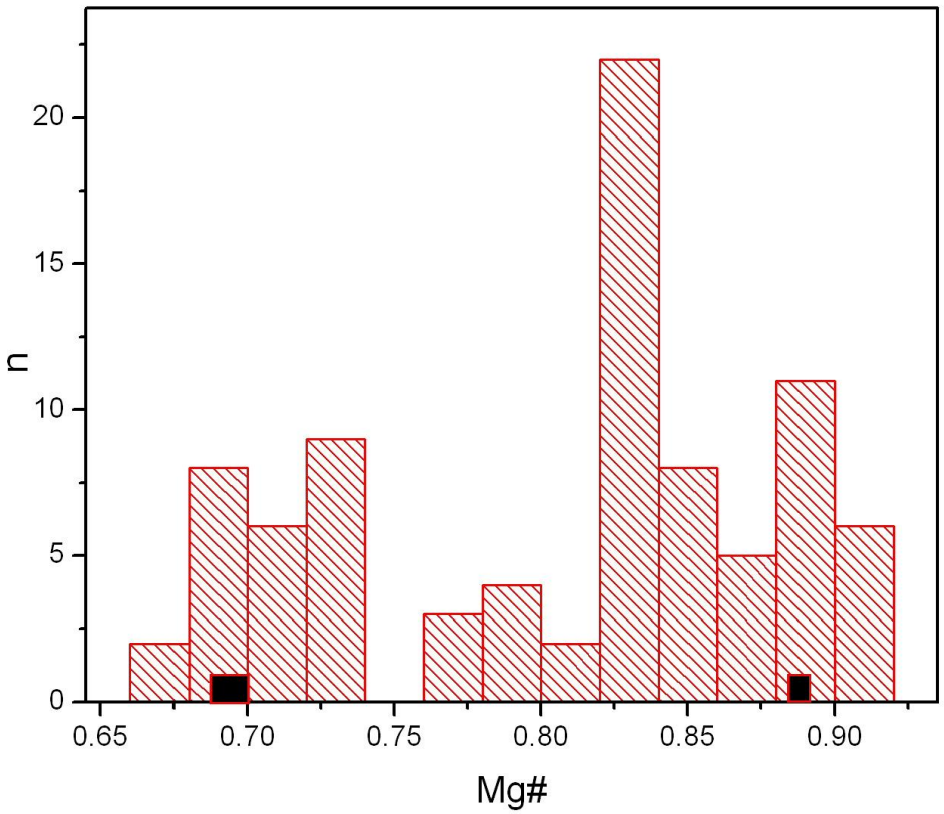

Figure 5A

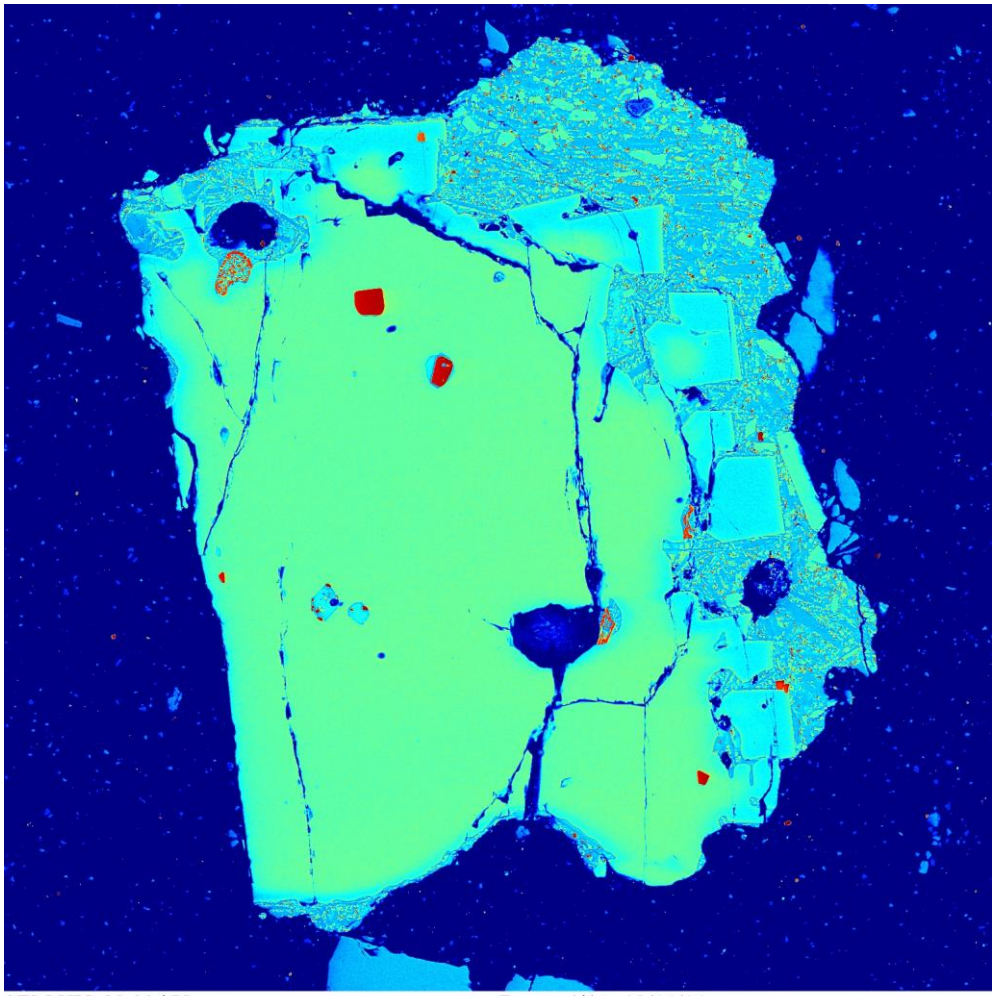

SEM HV: 20.00 kV
SEM MAG: 400 x
Nekrasov A.N.
Date(m/d/y): 10/14/14
View field: 954.0 µm
Det: BSE Detector + SE Detector

Figure 5B

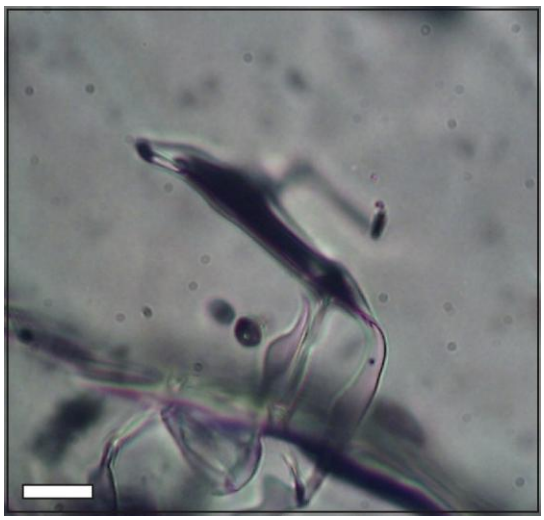

Figure 6

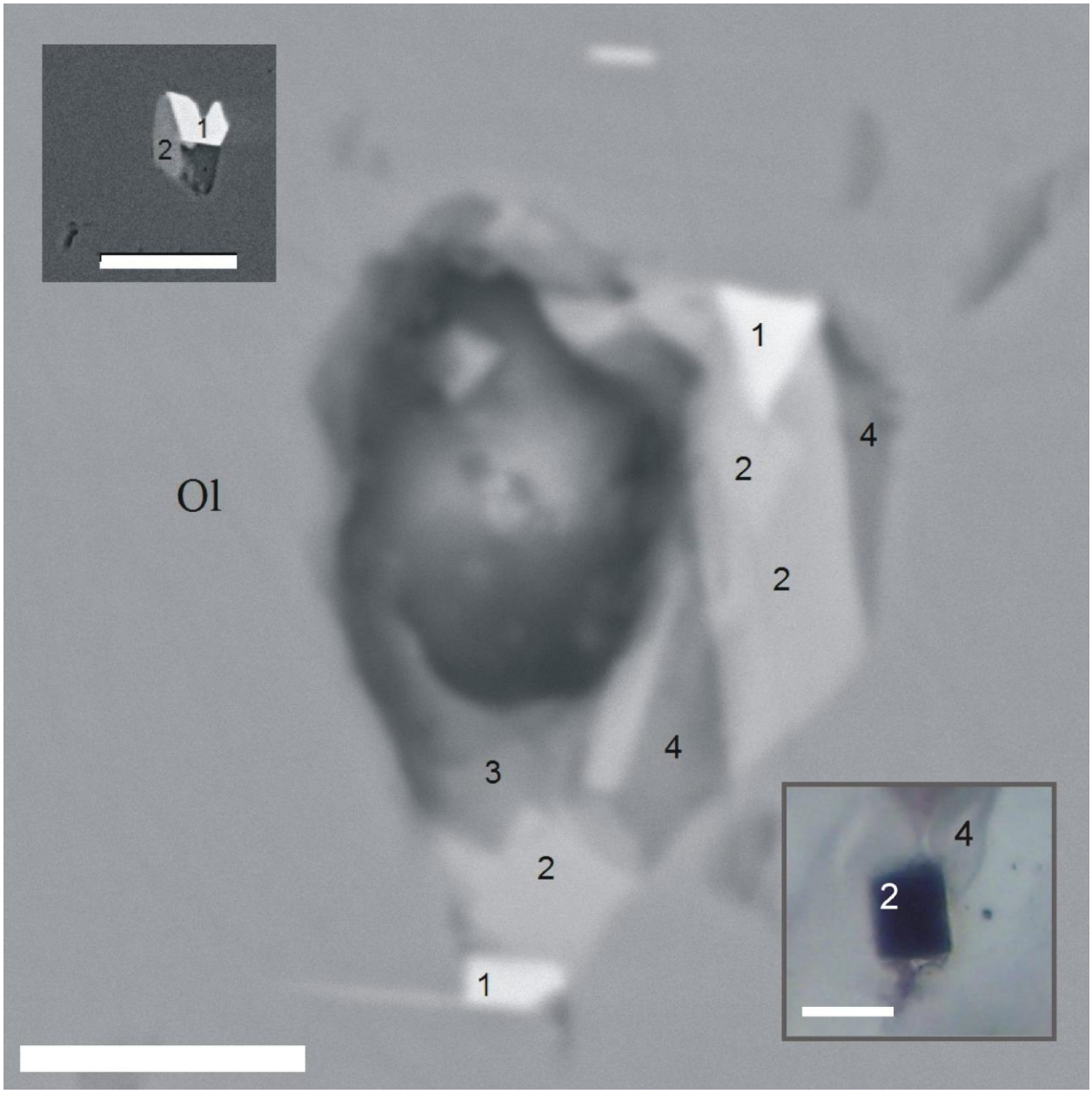

Figure 7

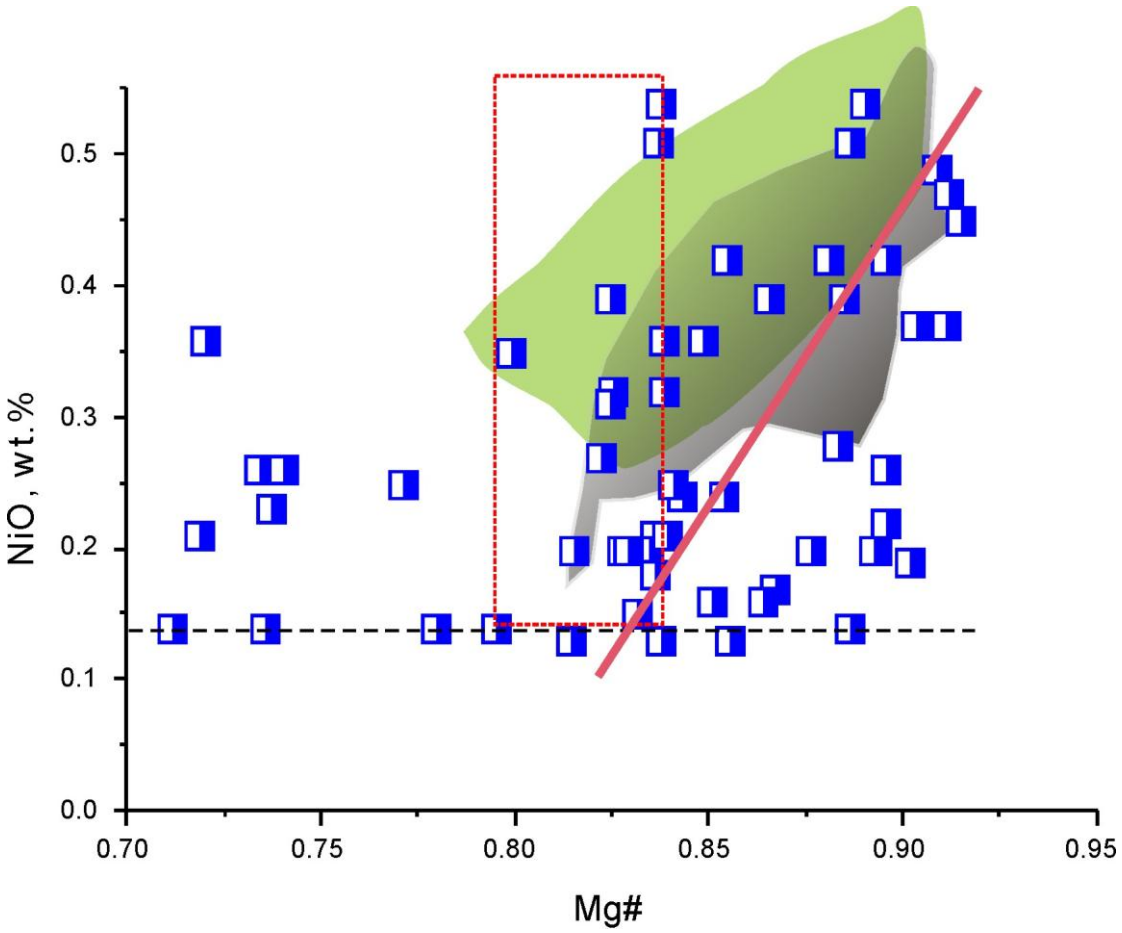

Figure 8

A

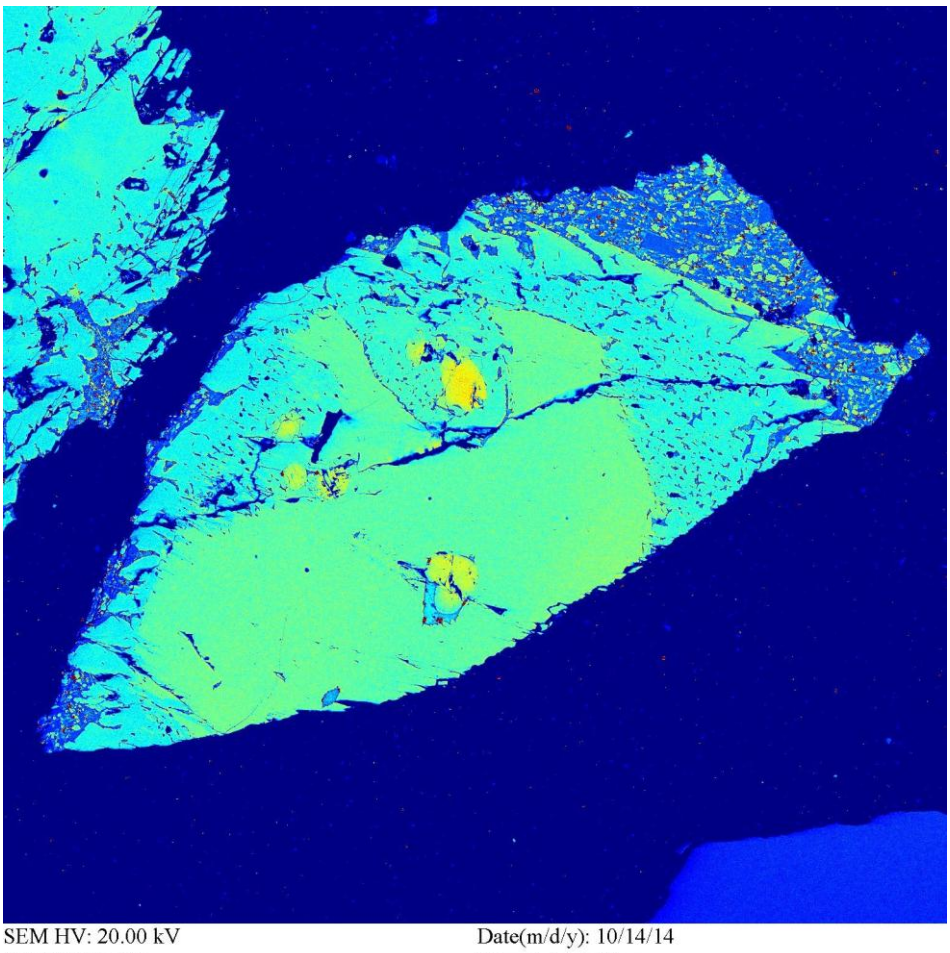

SEM HV: 20.00 kV
SEM MAG: 300 x
Nekrasov A.N.
Date(m/d/y): 10/14/14
View field: 1.27 mm
Det: BSE Detector + SE Detector

B

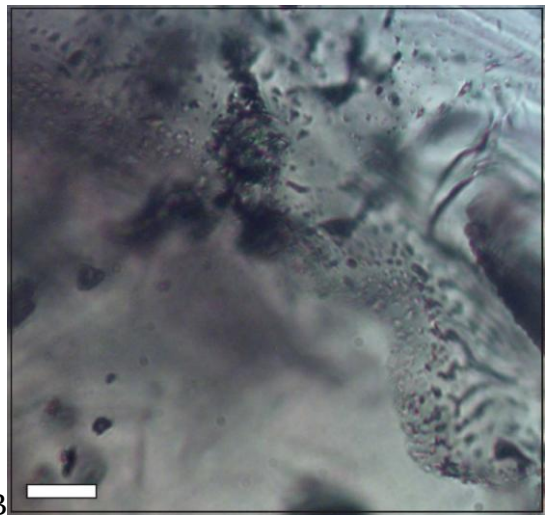

Figure 9

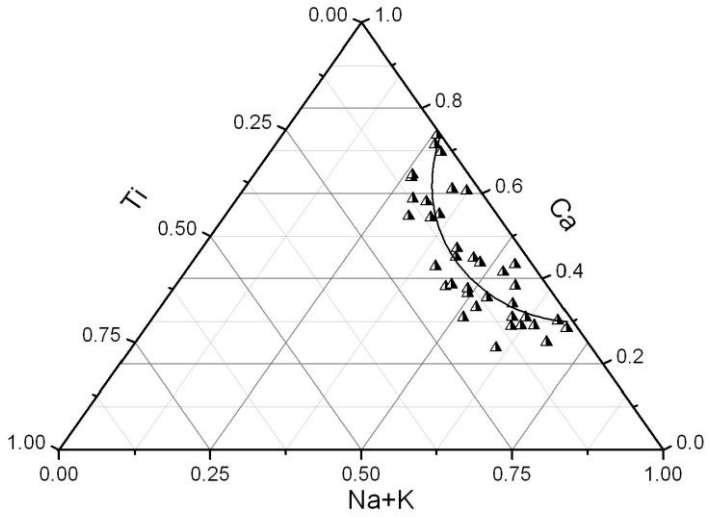
0.00
1.0
0.8
0.25
0.6
Ti
Ca
0.50
0.4
0.75
0.2
1.00
0.0
0.00
0.25
0.50
0.75
1.00
Na+K

A

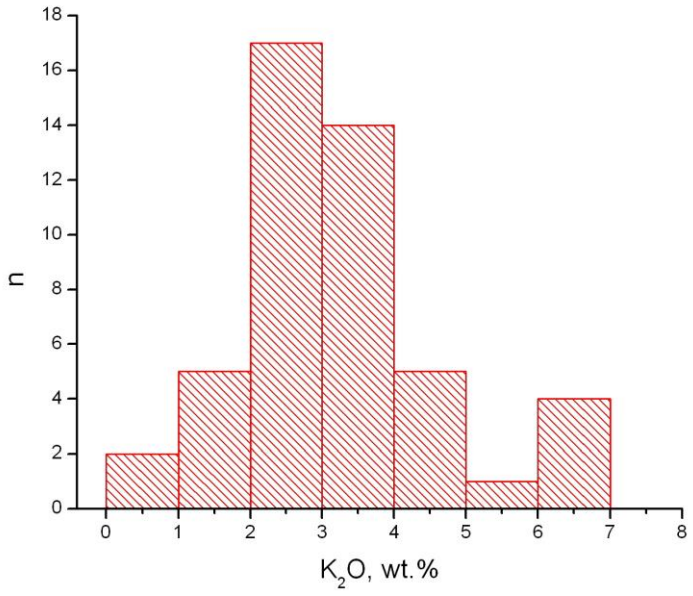
18
16
14
12
10
n
8
6
4
2
0
0
1
2
3
4
5
6
7
8
K2O, wt.%

B

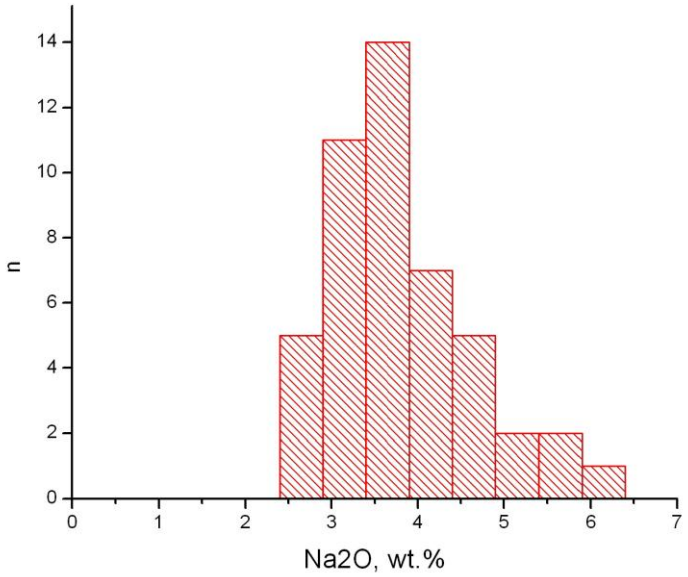
n
Na2O, wt.%
0
2
4
6
8
10
12
14
0
1
2
3
4
5
6
7

C

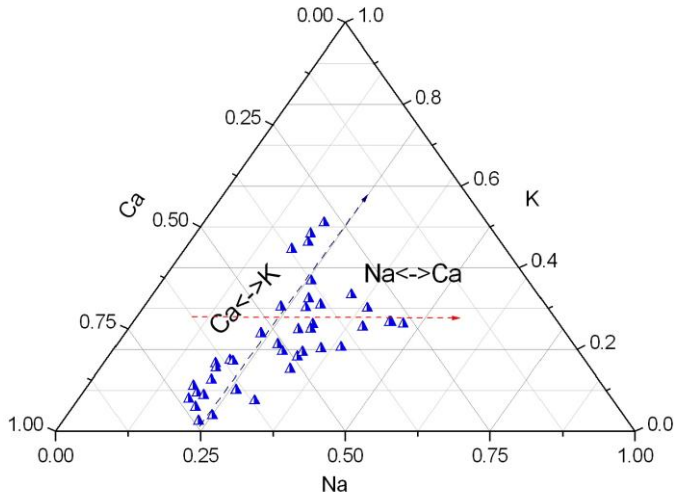
Ca
K
Na
Ca<->K
Na<->Ca
0.00
0.25
0.50
0.75
1.00
1.0
0.8
0.6
0.4
0.2
0.0

D

Figure 10

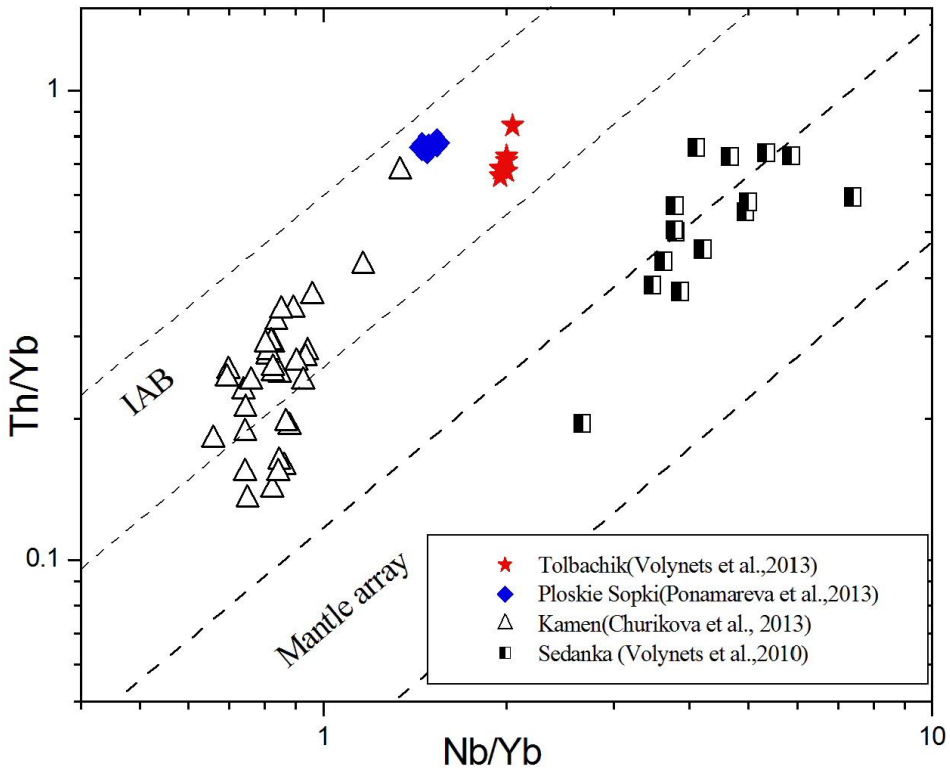
Th/Yb
Nb/Yb
1
0.1
1
10
IAB
Mantle array
Tolbachik(Volynets et al.,2013)
Ploskie Sopki(Ponamareva et al.,2013)
Kamen(Churikova et al., 2013)
Sedanka (Volynets et al.,2010)

Figure 11

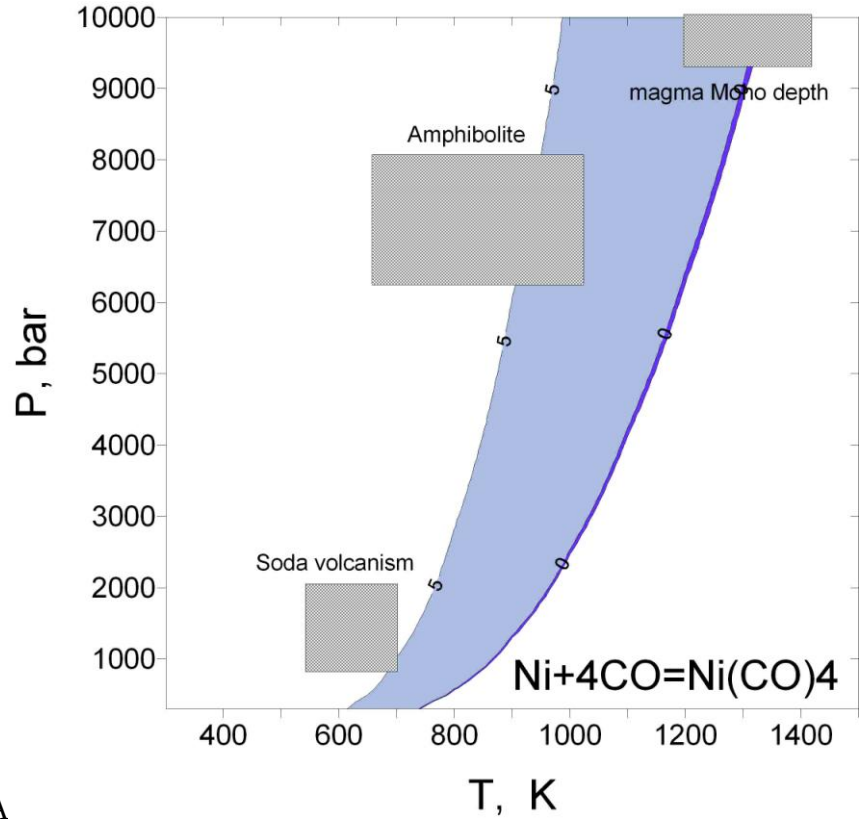
10000
9000
8000
7000
6000
5000
4000
3000
2000
1000
P, bar
400
600
800
1000
1200
1400
T, K
magma Moho depth
Amphibolite
Soda volcanism
5
5
5
0
0
Ni+4CO=Ni(CO)4

A

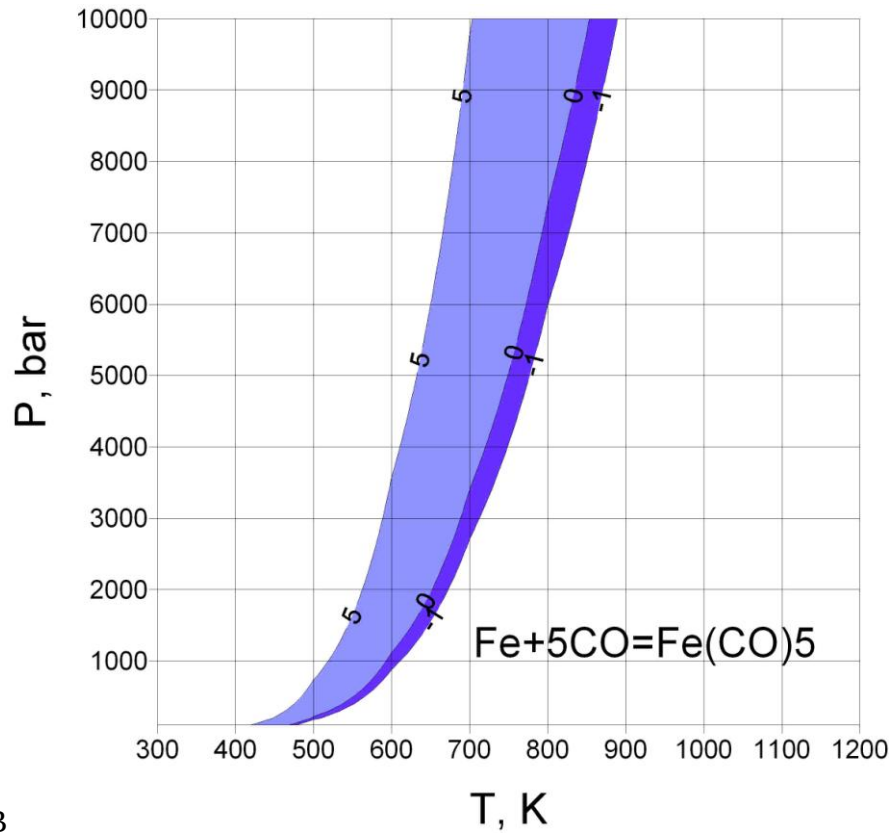
10000
9000
8000
7000
6000
5000
4000
3000
2000
1000
P, bar
300
400
500
600
700
800
900
1000
1100
1200
T, K
5
5
5
0
0
.1
.1
.1
Fe+5CO=Fe(CO)5

B

Figure 12

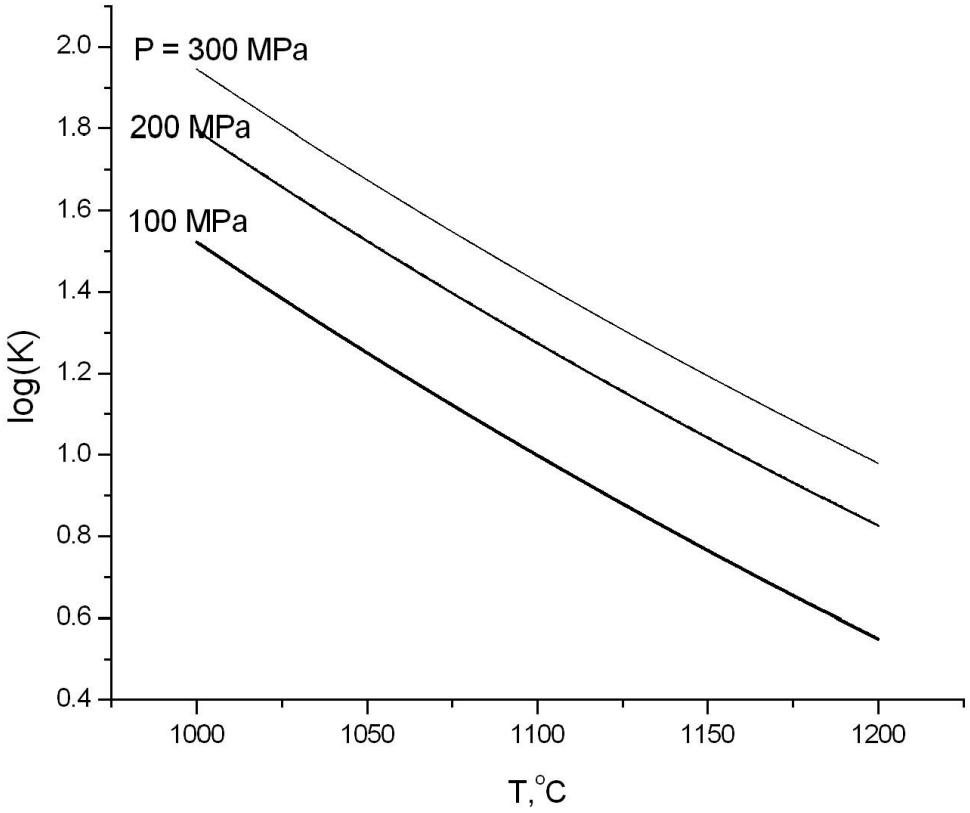
P = 300 MPa
200 MPa
100 MPa
log(K)
2.0
1.8
1.6
1.4
1.2
1.0
0.8
0.6
0.4
1000
1050
1100
1150
1200
T,°C

Figure 13

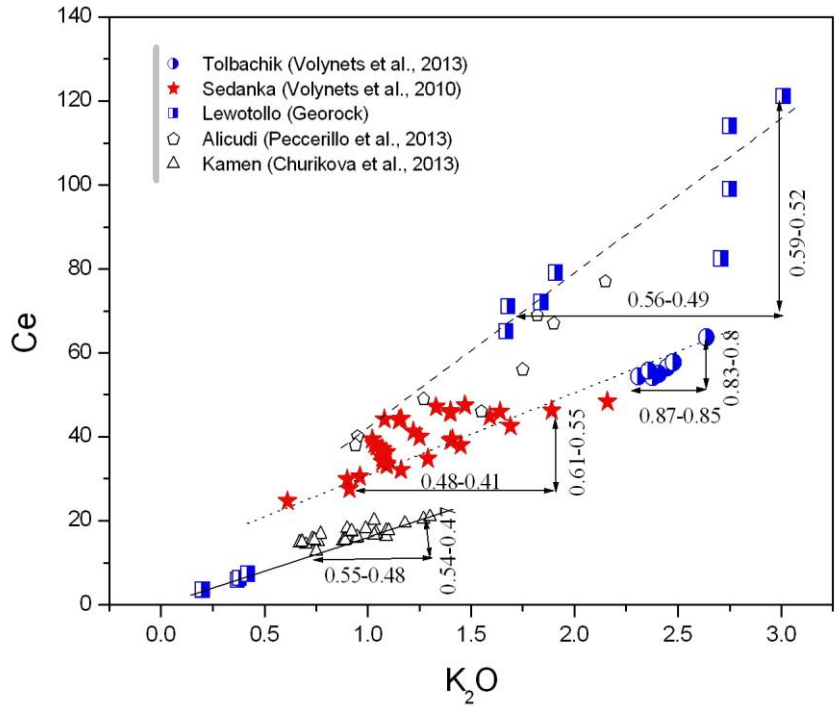
Tolbachik (Volynets et al., 2013)
Sedanka (Volynets et al., 2010)
Lewotollo (Georock)
Alicudi (Peccerillo et al., 2013)
Kamen (Churikova et al., 2013)
Ce
K2O
0.59-0.52
0.56-0.49
0.83-0.8
0.87-0.85
0.61-0.55
0.48-0.41
0.54-0.47
0.55-0.48

A

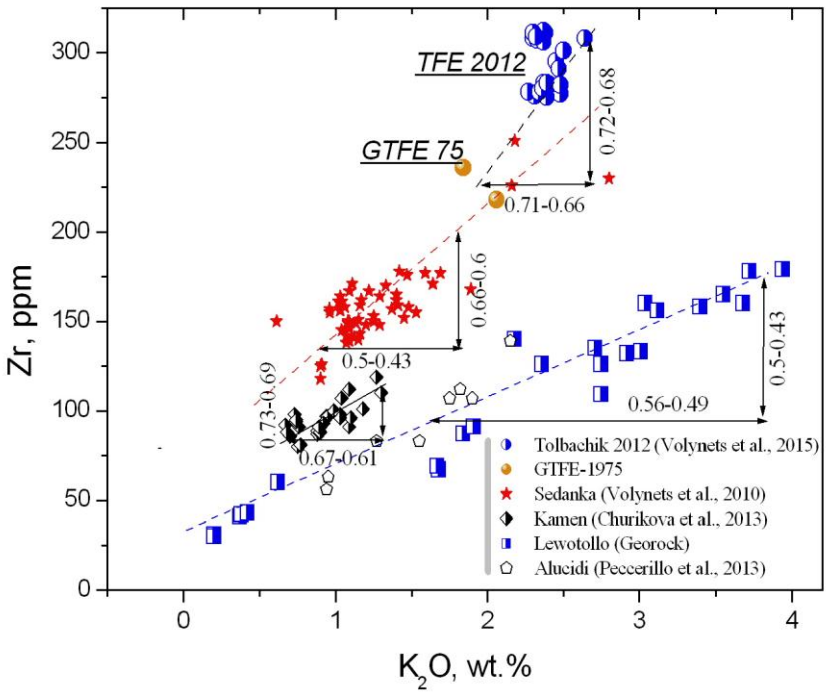
TFE 2012
GTFE 75
0.72-0.68
0.71-0.66
0.66-0.6
0.5-0.43
0.73-0.69
0.67-0.61
0.56-0.49
0.5-0.43
Tolbachik 2012 (Volynets et al., 2015)
GTFE-1975
Sedanka (Volynets et al., 2010)
Kamen (Churikova et al., 2013)
Lewotollo (Georock)
Alucidi (Peccerillo et al., 2013)
Zr, ppm
K2O, wt.%

B

Table 1 Compositions of the studied samples

sample	SiO_2	TiO_2	Al_2O_3	MgO	CaO	FeO	Na_2O	K
Tolb-1	51.2	2.1	16.3	3.8	7.6	10.5	3.6	2
Tolb-2	52.3	1.90	17.3	3.6	8.1	9.5	3.9	2
Bomb-1941	50.8	1.24	14.9	8.8	9.78	9.8	2.8	1
MIs average**	56.7±3.3	1.6 ±0.8	18.5±4.4	1.7±1.0	8.3±3.3	4.3±2.0	4.2±0.9	2.7
Lava 2012-2013*	52.3 ±1.3	1.9±1.1	16.1±0.3	3.8±0.4	7.2±0.3	10.4±1.2	3.6±0.2	2.4
GTFE-1975 North breach	49.69 ±0.62	1.03 ±0.09	13.26 ±0.35	9.97± 0.57	11.90 ± 0.43	9.64± 1.25	2.39± 0.11	0. 0
GTFE-1975 South breach	50.64 ±0.63	1.62 ±0.12	16.56 ±0.62	5.95 ±0.57	8.84 ±0.86	9.91 ±1.39	3.39 ±0.18	1 ±

* analysis of high aluminum basalt of 2012-2013 Tolbachik eruption from [Volynets et al., 2013], Tolb-1 dense lava, Tolb-2 vesiculated lava, Tolb-3 volcanic bomb of 1941 Tolbachik eruption, ** - average over 26 different melt inclusion analysis in mafic minerals from sample Tolb-3. .

Table 2. Compositions of the minerals and MIs from Tolbachik lava

	Garnet				Clinopyroxene						Olivine					
SiO2	37.82	39.3	37.84	29.02	50.85	50.95	50.83	50.95	51.99	53.05	36.98	39.16	37.9	39.75	40.34	43.48
TiO2	3.79	3.31	3.94	5.55	0.64	0.75	0.89	0.55	0.46	0.62	0.1	0.17	0.03	0.17	0.07	0.28
Al2O3	14.3	13.75	14.22	16.14	2.89	3.47	2.93	2.87	2.5	2.18	0.22	0.06	0	0.06	0.17	0.27
Cr2O3	0	0	0	0.14	0.48	0.57	0.4	0.33	0.05	0.25	0	0	0	0	0	0
FeO	9.76	9.07	9.47	18.14	9.09	9.4	9.81	6.02	5.8	6.27	25.00	23.95	23.35	10.08	14.72	14.35
MnO	0	0.3	0.08	0.18	0.27	0.21	0.31	0.15	0	0.02	0.41	0.54	0.55	0.26	0.34	0.14
NiO	0	0	0	0	0	0	0	0	0	0	0.36	0.23	0.26	0.54	0.51	0.54
MgO	8.63	9.47	8.89	12.91	15.58	15.41	15.36	16.33	16.73	17.54	36.51	38.81	38.52	49.34	44.7	43.48
CaO	24.3	22.64	24.3	16.78	18.26	18.12	18.91	20.99	21.11	20.95	0.29	0.27	0.22	0.25	0.06	0.25
Na2O	0.42	0.6	0.35	0.67	0.39	0.5	0.42	0.39	0.26	0.25	0	0	0	0	0	0
K2O	0.14	0.16	0.02	0.02	0.14	0.01	0	0	0	0	0	0	0	0	0	0
sum	99.16	98.6	99.11	99.55	98.59	99.39	99.86	98.58	98.9	101.13	99.87	103.19	100.83	100.45	100.91	102.79
Si	2.891	3.000	2.886	2.288	1.910	1.897	1.888	1.891	1.921	1.918	0.977	0.994	0.982	0.971	1.006	1.072
Al iv	0.109	0.000	0.114	0.712	0.090	0.103	0.112	0.109	0.079	0.082	0.000	0.000	0.000	0.000	0.000	0.000
Al vi	1.207	1.262	1.192	0.834	0.038	0.049	0.016	0.017	0.030	0.011	0.007	0.002	0.000	0.002	0.005	0.008
Ti	0.218	0.190	0.226	0.329	0.018	0.021	0.025	0.015	0.013	0.017	0.002	0.003	0.001	0.003	0.001	0.005
Cr	0.000	0.000	0.000	0.009	0.014	0.017	0.012	0.010	0.001	0.007	-	-	-	-	-	
Fe3+	0.499	0.474	0.504	0.724	0.030	0.032	0.065	0.080	0.040	0.047	0.036	0.003	0.035	0.051	0.000	0.000
Fe2+	0.125	0.105	0.100	0.472	0.255	0.261	0.240	0.107	0.139	0.142	0.516	0.505	0.471	0.155	0.307	0.296
Mn	0.000	0.019	0.005	0.012	0.009	0.007	0.010	0.005	0.000	0.001	0.009	0.012	0.012	0.005	0.007	0.003
Mg	0.983	1.078	1.011	1.517	0.872	0.855	0.850	0.904	0.922	0.945	1.437	1.469	1.488	1.796	1.662	1.598
Ni	0.000	0.000	0.000	0.000	0	0	0	0	0	0	0.008	0.005	0.005	0.011	0.010	0.011
Ca	1.990	1.852	1.986	1.417	0.735	0.723	0.752	0.835	0.836	0.812	0.008	0.007	0.006	0.007	0.002	0.007
Na	-	-	-	-	0.028	0.036	0.030	0.028	0.019	0.018	0.000	0.000	0.000	0.000	0.000	0.000
Total	8.024	7.979	8.024	8.314	4.000	4.000	4.000	4.000	4.000	4.000	3.000	3.000	3.000	3.000	3.000	3.000
Mg#	0.61	0.65	0.63	0.56	0.75	0.74	0.74	0.83	0.84	0.83	0.72	0.74	0.75	0.90	0.84	0.84
Fe^3/Fe^t	0.800	0.819	0.834	0.605	0.105	0.109	0.213	0.428	0.223	0.249	0.065	0.006	0.069	0.248	0.000	0.000

Table 2. (continued) Compositions of the glass inclusions in minerals from Tolbachik lava

oxides	MIs in Clinopyroxene						MIs in Olivine					
	Reaction zone		Low Mg				High Mg			Low Mg		
SiO_2	58.32	59.46	60.02	62.5	64.33	57.93	53.6	55.04	53.51	54.27	54.94	54.63
TiO_2	2.35	2.35	1.22	1.01	0.86	2.43	0.81	2.95	1.9	1.91	1.79	1.64
Al_2O_3	15.52	15.63	18.46	18.45	18.74	15.29	19.02	13.64	15.54	14.47	14.92	15.37
Cr_2O_3	0.14	0	0.03	0.09	0.04	0	0.79	0.25	0.54	0.01	0.04	0
FeO	5.4	5.18	1.16	1.66	1.47	3.72	2.09	8.1	5.86	6.32	6.33	5.48
MnO	0.13	0.08	0.04	0.07	0.05	0.15	0.03	0.18	0	0.5	0.13	0.4
NiO	0.23	0	0	0.08	0.01	0.04	0	0.13	0.03	0	0.02	0.12
MgO	2.83	2.78	0.86	1.23	0.58	2.04	0.59	1.4	2.97	1.49	1.35	1.27
CaO	5.76	5.89	3.99	4.29	3.23	3.66	5.88	5.17	8.44	9.15	10.24	9.5
Na_2O	3.71	2.92	4.7	5.35	5.63	2.7	4.77	3.55	3.77	3.2	3.15	3.45
K_2O	3.12	3.27	2.97	4.14	3.14	6.61	2.69	5.06	3.82	2.59	2.46	2.66
P_2O_5	1.01	1.33	0.98	0.94	0.78	1.78	0.39	0.85	0.73	0.73	1.05	0.66
SO_3	0.2	0	0.38	0.42	0.31	0	0.89	0.15	0.12	0.22	0.04	0
Cl	0.13	0.12	0.09	0.09	0.1	0.14	0.21	0.23	0.09	0.05	0.1	0
F	nd	nd	nd	nd	nd	0.28	0.2	0	0	0	0	0.19
sum	98.85	99.01	94.9	100.32	99.27	96.77	91.96	96.7	97.32	94.84	96.44	95.17

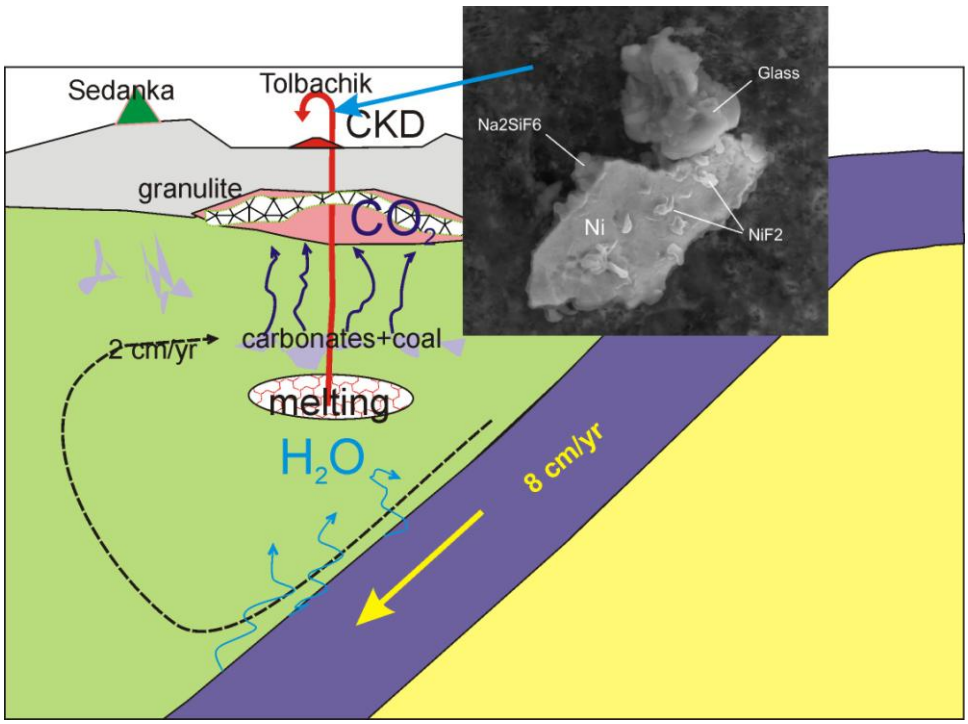

Graphical abstract

Highlights

- In 2012-2013 Tolbachik eruption aerosols native Ni and PGE were found.
- Both potassic nature of Tolbachik lavas and native metals in aerosols are attributed to the action of dry reduced carbonic fluid. Thermodynamic modeling predicts that Ni can be highly volatile at high PT as $Ni(CO)_4$.